APPENDIX A-M

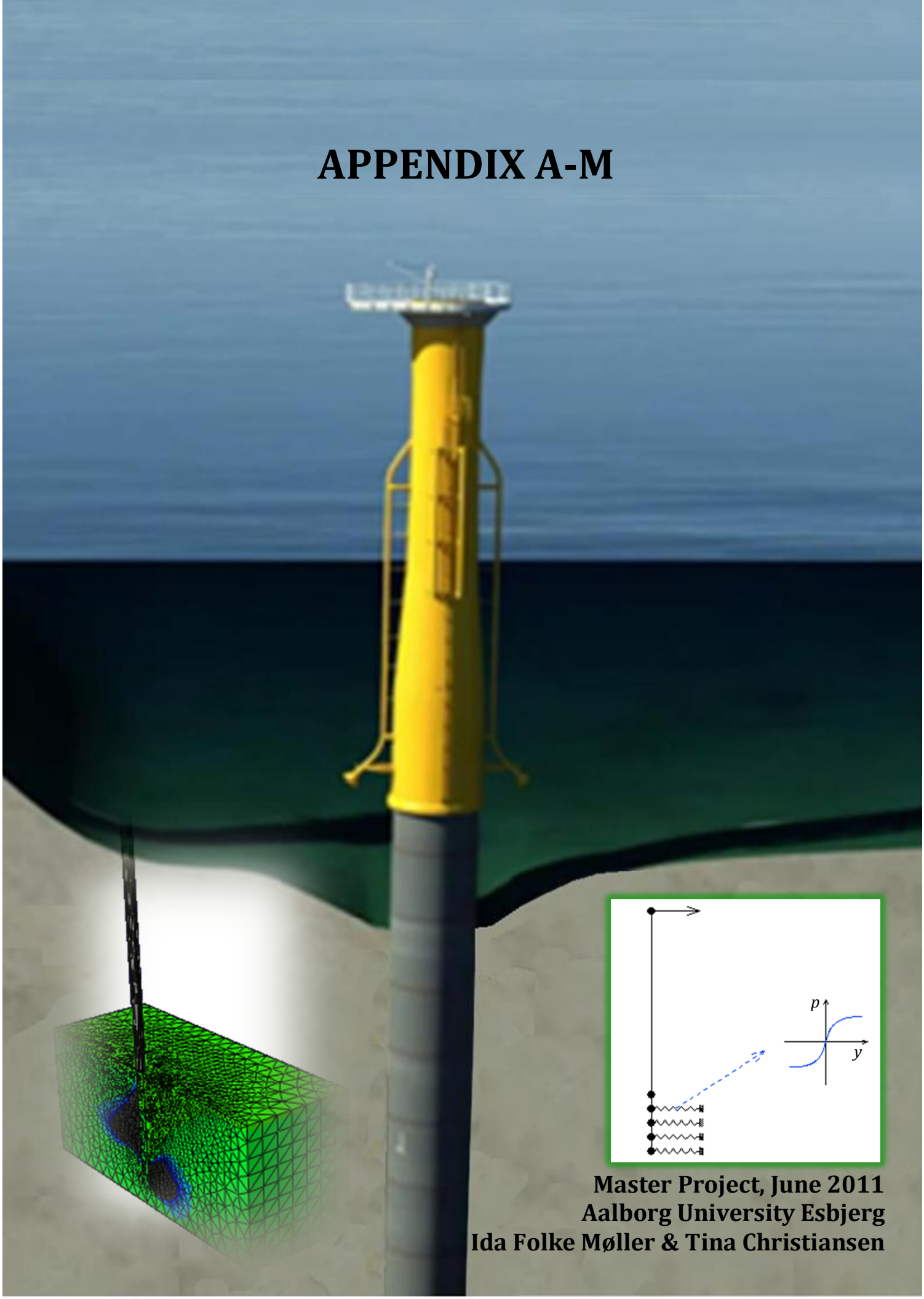

Master Project, June 2011
Aalborg University Esbjerg
Ida Folke Møller & Tina Christiansen

Contents

A. Pile cross section control

During both the p-y experiments and the static experiments the submerged part of the pile will be subjected to large pressures from the soil. In this section an Abaqus model of the 0.1 m segment used in the p-y experiments is examined to ensure that no plastic deformations of the pile or the pile segment will occur during the experiments.
In the p-y experiments the bottom of the pile segment is placed in a depth of 0.45 m and the bottom of the pile in the static experiments is placed 0.4 m below the ground surface. Therefore the pile segment will be subjected to the largest soil pressures. As the cross section of this and the pile is the same the stresses in the pile segment are examined for the maximum soil pressure.

A.1 Model geometry

The pile segment used in the p-y experiments is modelled in Abaqus. The model exploits symmetry around one axis, which means that half of the cross section is modelled. Figure A.1 shows the model of the pile segment.

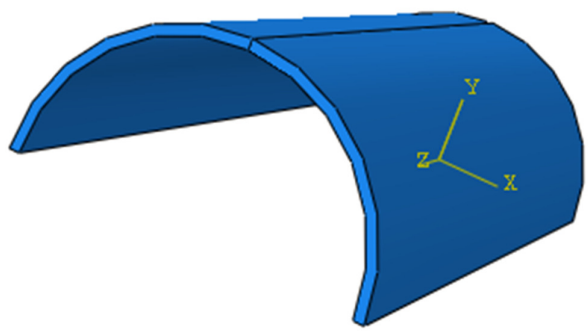

Figure A.1: Abaqus model of the pile segment with a height of 0.1 m, an outer diameter of 0.0508 m and a thickness of 0.0015 m. Symmetry around one axis is exploited.

A.2 Boundary conditions

Figure A.2 shows the boundary conditions for the model.

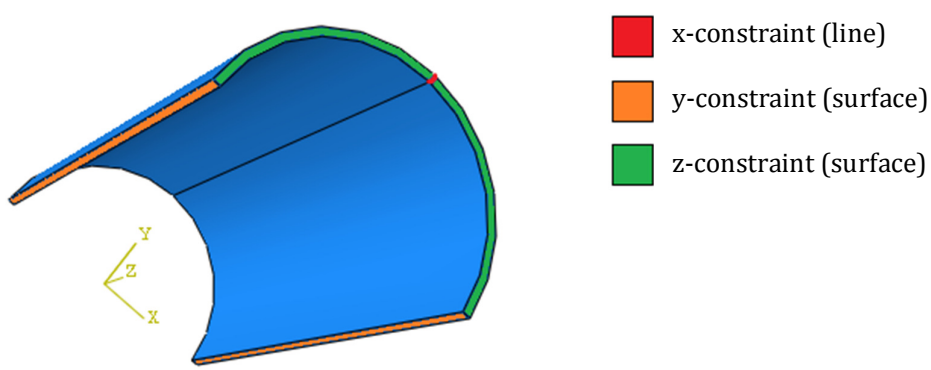

Figure A.2: Boundary conditions for the model of the pile segment.

A.3 Load

The way the load is applied should simulate the way the earth pressure loads the pile segment and the pile. This is obtained by creating a cape around the pile which has very little stiffness. This means that the load is transferred directly to the pile through the cape material. On top of this cape the load from the earth pressure can be applied as a surface load.

The cape is merged with the pile segment and the model with the cape is shown in Figure A.3.

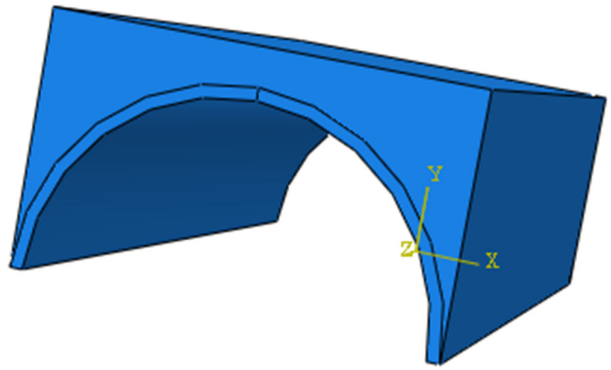

Figure A.3: Merged model of the pile segment. The material for transferring the load has a stiffness that is 10^{-11} less that the stiffness of the pile segment.

The maximum load that the pile segment can be subjected to is determined by the p-y curve for the sand used in the experiments 0.45 m below the ground surface. Figure A.4 shows this p-y curve.

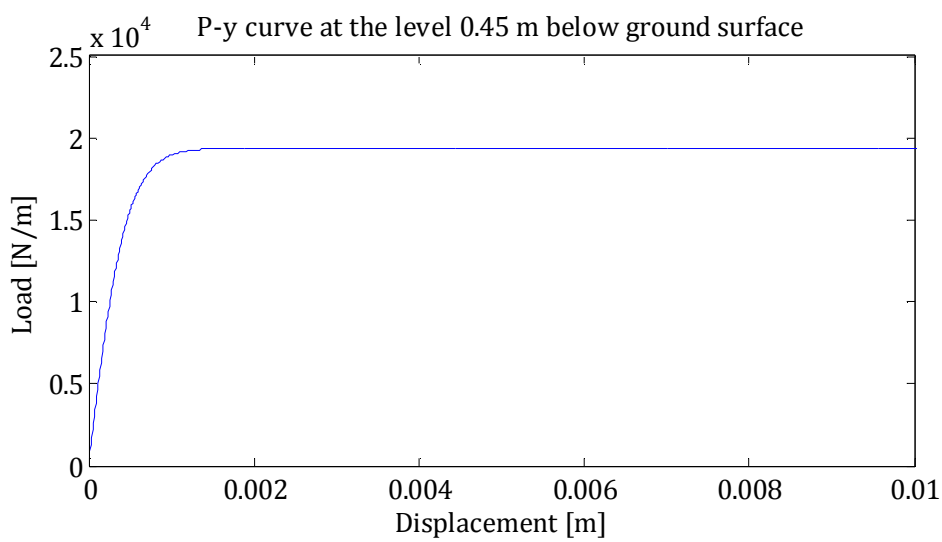

Figure A.4: P-y curve at the level 0.45 m below the ground surface.

The maximum load on the p-y curve is approximately 20,000 N/m. On the safe side this load is assumed to be the load along the entire segment of 0.1 m. The load is applied as a surface load on the cape. This surface load is:

$$P = \frac{20{,}000\ N/m}{0.0508\ m} = 4 \cdot 10^5\ N/m^2 \tag{A.1}$$

A.4 Mesh

The model is meshed with second order tetrahedron elements with a size of 0.003 m. Figure A.5 shows the mesh.

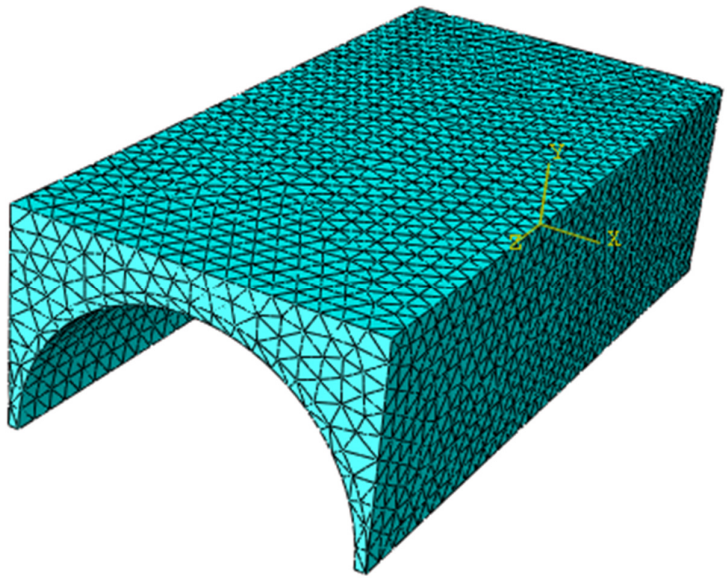

Figure A.5: Mesh for the model. The elements are second order tetrahedron elements.

A.5 Results

The model is solved and the Von Mises stresses are shown in Figure A.6.

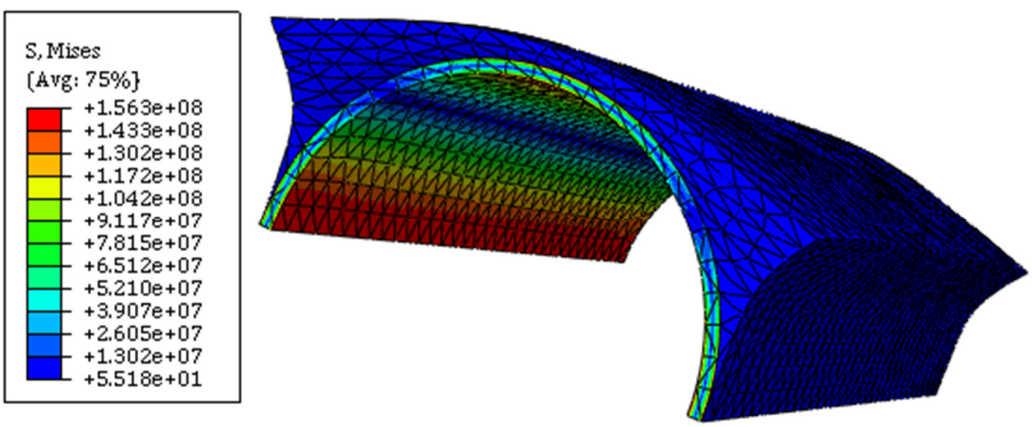

Figure A.6: Von Mises stresses when solving the model.

The figure shows that the maximum Von Mises stress is 156 MPa which is less than the yield stress of the steel of 235 Mpa. Therefore it is assessed that the pile will not undergo plastic deformation during the p-y experiments or the static experiments.

B. Friction in p-y experiments

The magnitude of the friction between the pile segment and the sand on the top and bottom surfaces is determined in this section. As the pile segment is hollow both friction between steel and sand and friction between sand and sand will be present, see Figure B.1.

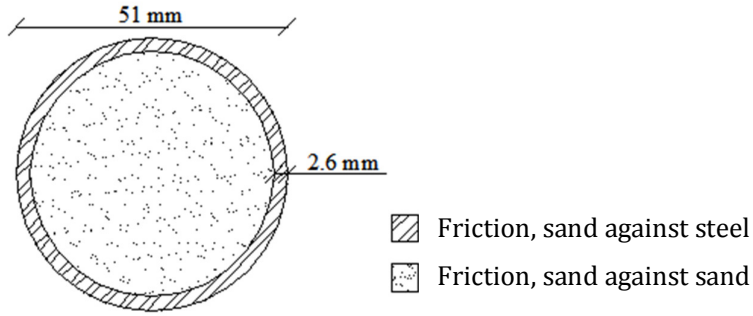

Figure B.1: Illustration of types of friction on the top and bottom of the pile segment.

The coefficient of friction between sand and steel is set to 0.5 as the sand has a relatively high density.
The coefficient of friction between sand and is set to 0.6.

The friction force, F_f, is determined:

$$F_f = \mu \cdot F_N \tag{B.1}$$

Where

μ is the coefficient of frictio

F_N is the normal force determined as the normal force from the sand above

For e = 0,1 m the normal force from the sand above the pile segment is:

$$F_f = \mu \cdot F_N F_{N,stål,0.1} = 0.05\ m \cdot (\pi \cdot (0.0255\ m)^2 - \pi \cdot (0.0229\ m)^2) \cdot 17540\ \frac{N}{m^3} = 0.03467\ N \tag{B.2}$$

And the mass of the sand inside the pile segment is:

$$F_{N,stål,0.1} = 0.05\ m \cdot \pi \cdot (0.0229\ m)^2 \cdot 17540\ \frac{N}{m^3} = 1.44\ N \tag{B.3}$$

The mass of the sand above the bottom part of the pile segment for all overburden pressures is shown in Table B-1.

e [m]	**Normal force, top, steel [N]**	**Normal force, bottom, steel [N]**	**Normal force, top, sand [N]**	**Normal force, bottom, sand [N]**
0.1	0.03467	0.104	1.44	4.33
0.2	0.104	0.173	4.33	7.22
0.3	0.173	0.243	7.22	10.11
0.4	0.243	0.312	10.11	13.0
0.5	0.312	0.381	13.0	15.89

Table B-1: Values of the normal force at different overburden pressures, e.

The total friction force is determined as the sum of the friction between sand and steel and the friction between sand and sand below and above the pile segment.

The friction force for e = 0.1 m is:

$$F_{f,0.1} = 0.5 \cdot (0.03467 + 0.104) + 0.6 \cdot (1.44 + 4.33) = 3.53\ N \tag{B.4}$$

The friction forces for all values of e are shown in Table B-2.

***e*[m]**	**0.1**	**0.2**	**0.3**	**0.4**	**0.5**
F_f [N]	3.53	7.07	10.61	14.14	17.68

Table B-2: Friction forces.

The values are less than 1 % of the ultimate resistances. Therefore the addition of the friction between the end surfaces is considered negligible.

C. Results of p-y experiments

During the p-y experiments the loads and the displacements are measured. The displacements are measured in two points outside of the box - one point below the centre of the test subject and one point above the centre of the test subject. The average of these two displacements is assumed to be the displacement at the centre of the test subject. The experiments are done at four different overburden pressures: *e* = 0.1 m, *e* = 0.2 m, *e* = 0.3 m and *e* = 04 m. Where the distance, *e*, is the distance between the top of the sand and the centre of the test subject. The load-displacement curves for the p-y experiments are shown in Figure C.1 to Figure C.12.

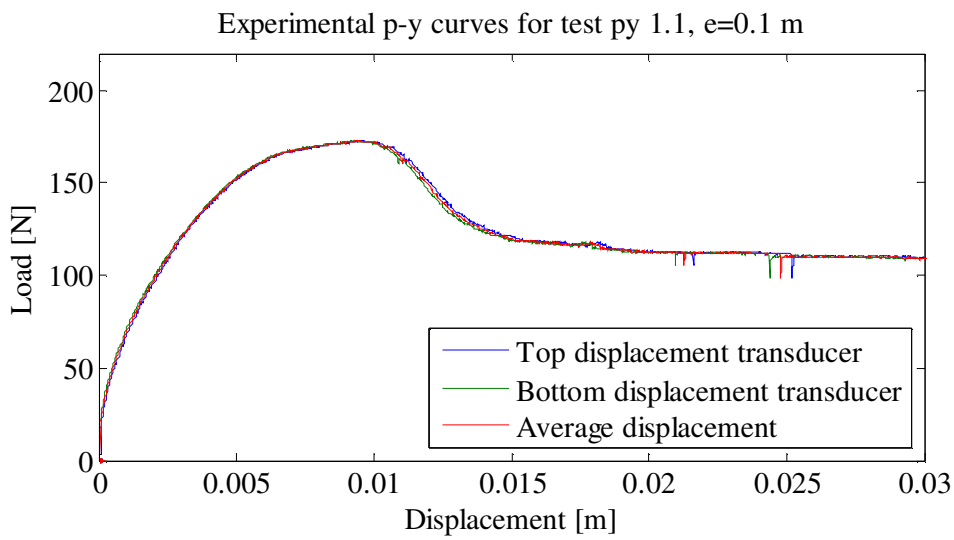

Figure C.1: Load-displacement curves for p-y experiment py 1.1 with e = 0.1 m.

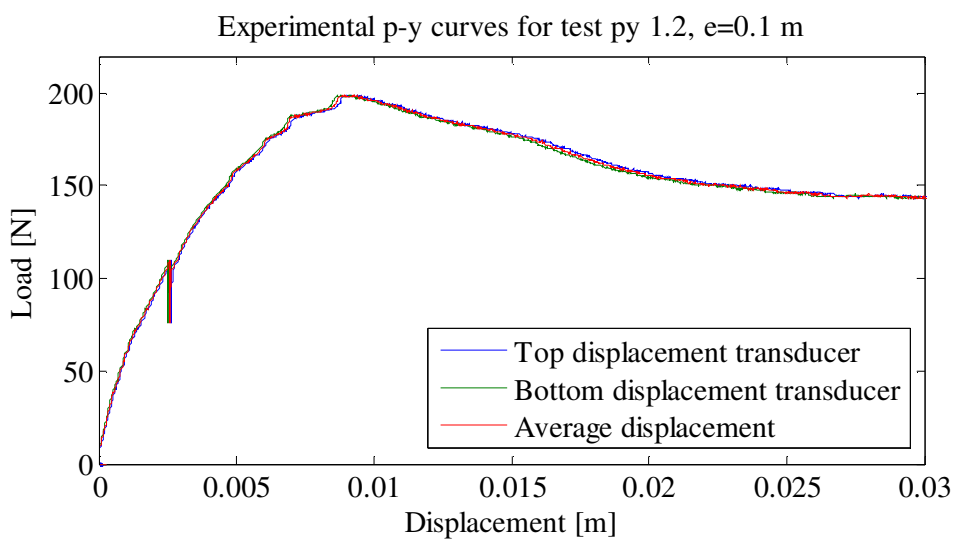

Figure C.2: Load-displacement curves for p-y experiment py 1.2 with e = 0.1 m.

Figure C.1 to Figure C.3 show some sudden drops in the force. This is caused by someone touching the box or the force transducer during the experiments. Therefore the drops should be disregarded when reviewing the results.

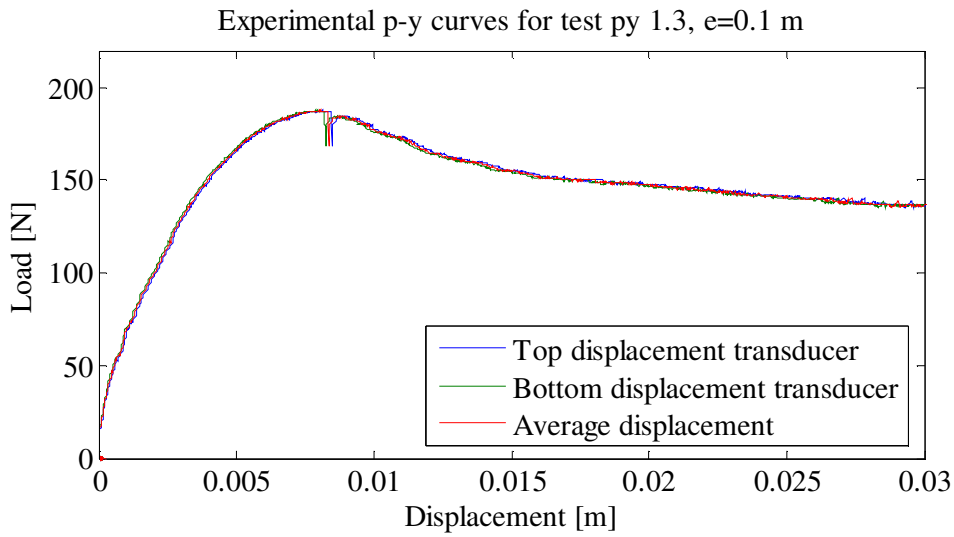

Figure C.3: Load-displacement curves for p-y experiment py 1.3 with e = 0.1 m.

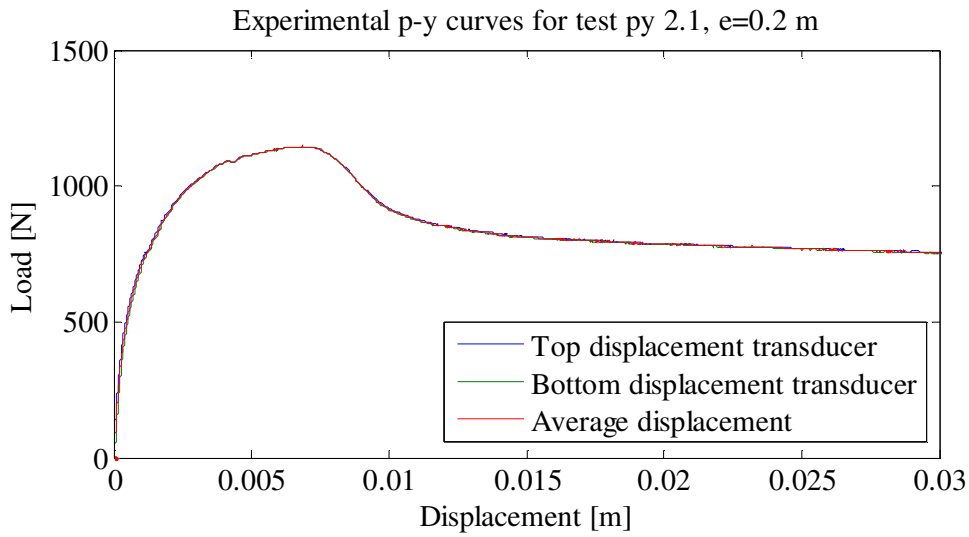

Figure C.4: Load-displacement curves for p-y experiment py 2.1 with e = 0.2 m.

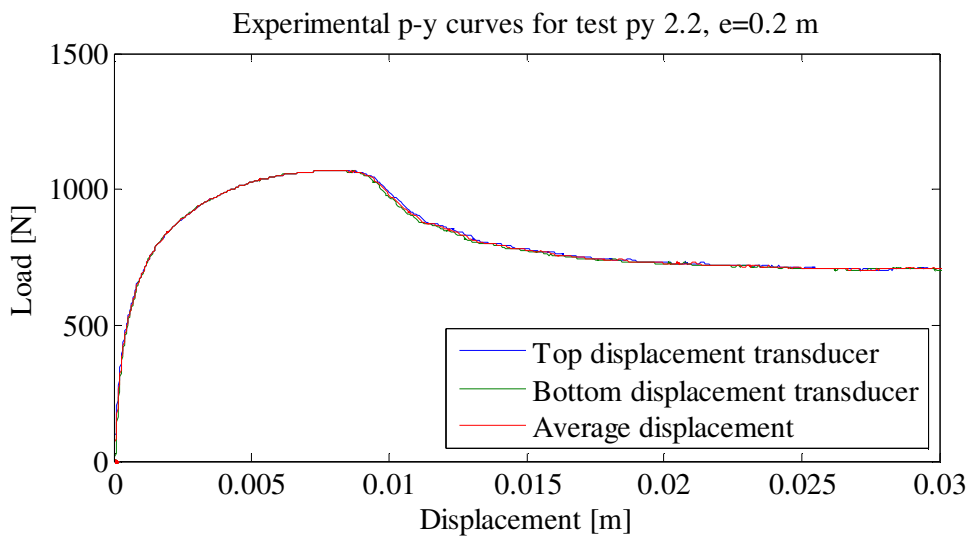

Figure C.5: Load-displacement curves for p-y experiment py 2.2 with e = 0.2 m.

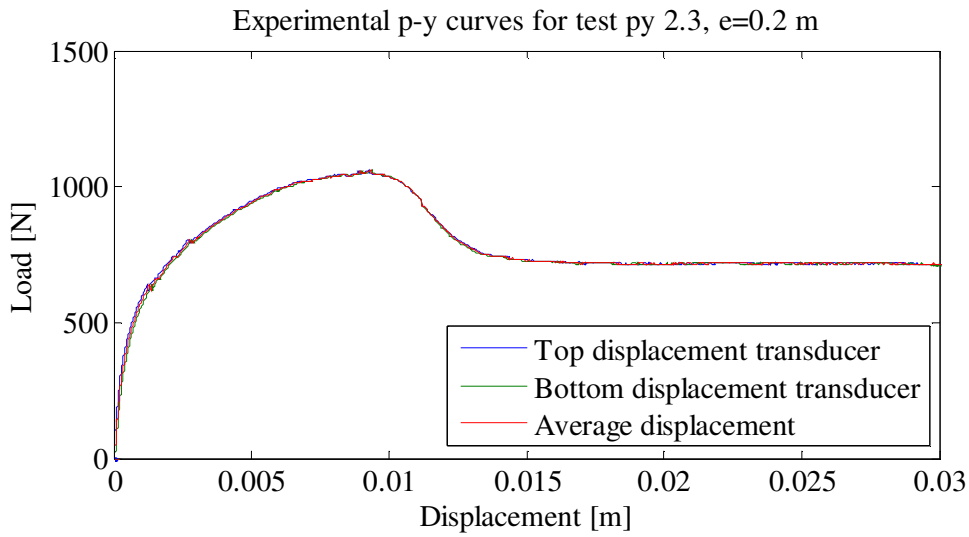

Figure C.6: Load-displacement curves for p-y experiment py 2.3 with e = 0.2 m.

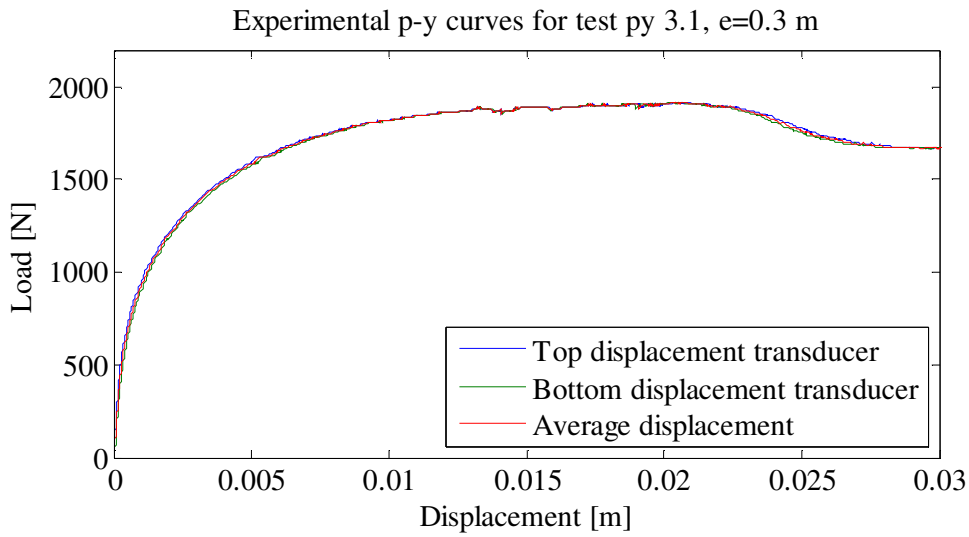

Figure C.7: Load-displacement curves for p-y experiment py 3.1 with e = 0.3 m.

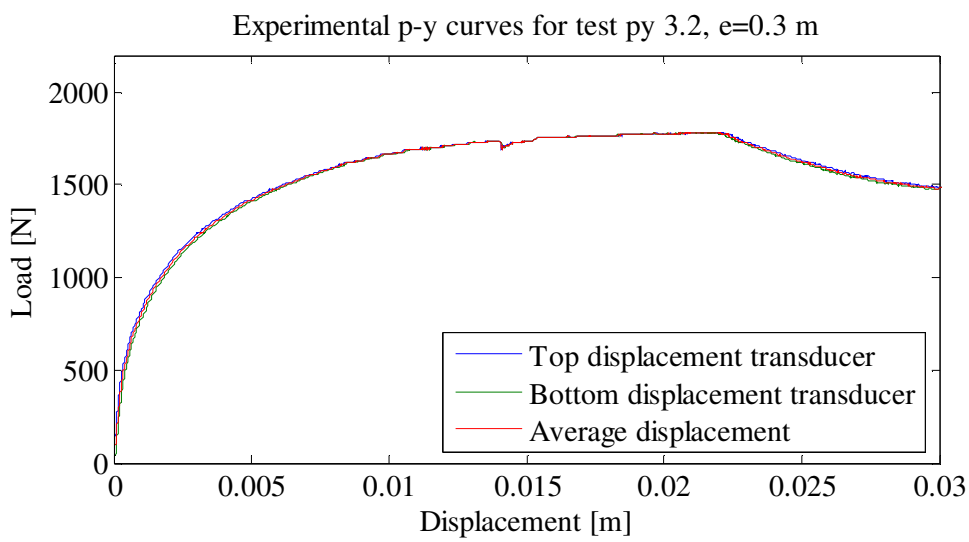

Figure C.8: Load-displacement curves for p-y experiment py 3.2 with e = 0.3 m.

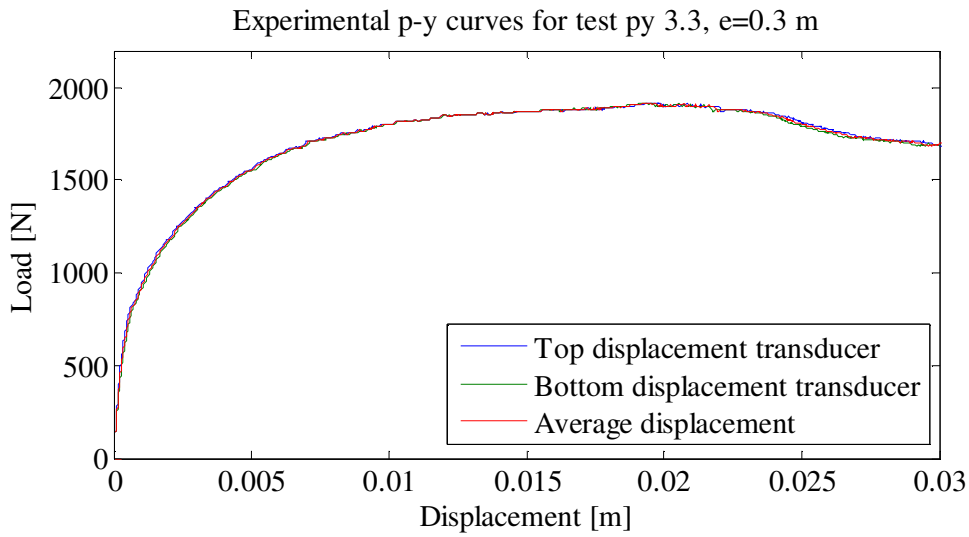

Figure C.9: Load-displacement curves for p-y experiment py 3.3 with e = 0.3 m.

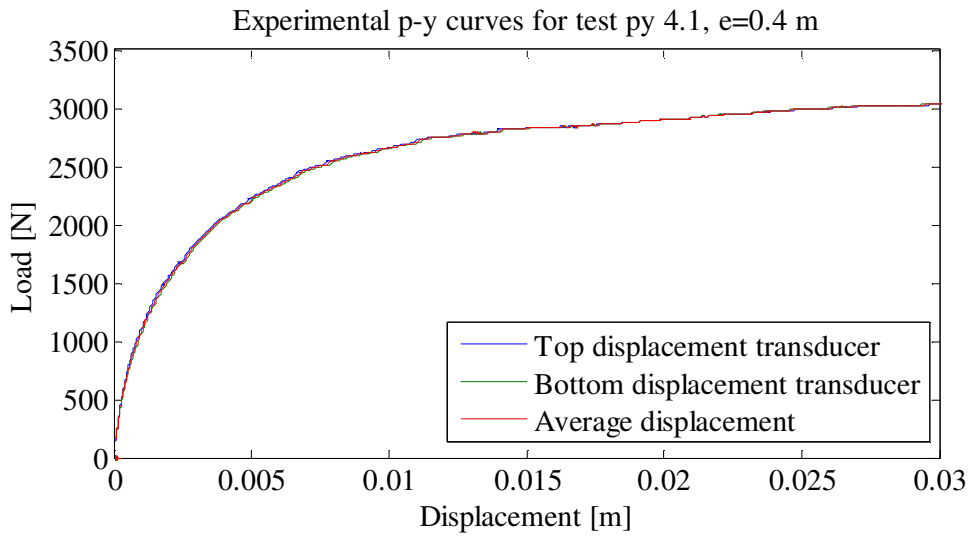

Figure C.10: Load-displacement curves for p-y experiment py 4.1 with e = 0.4 m.

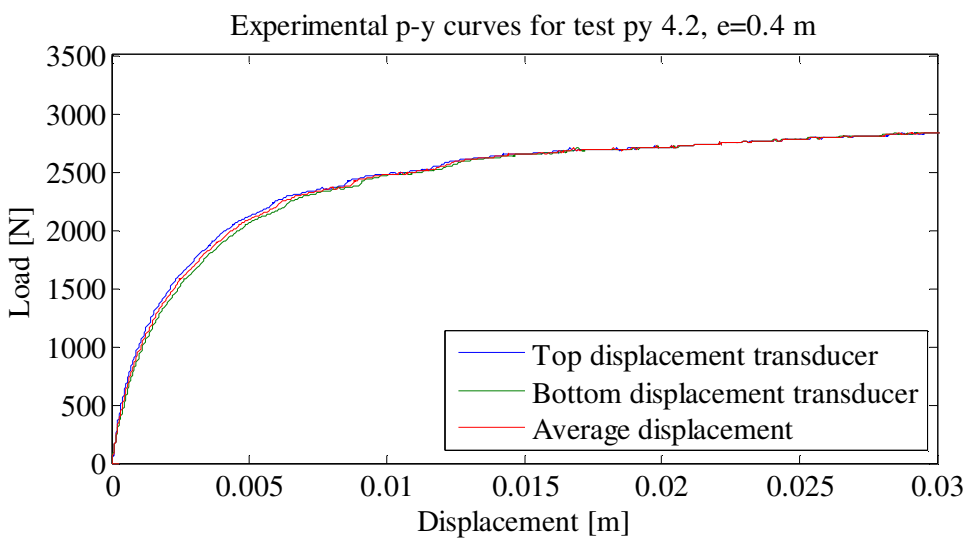

Figure C.11: Load-displacement curves for p-y experiment py 4.2 with e = 0.4 m.

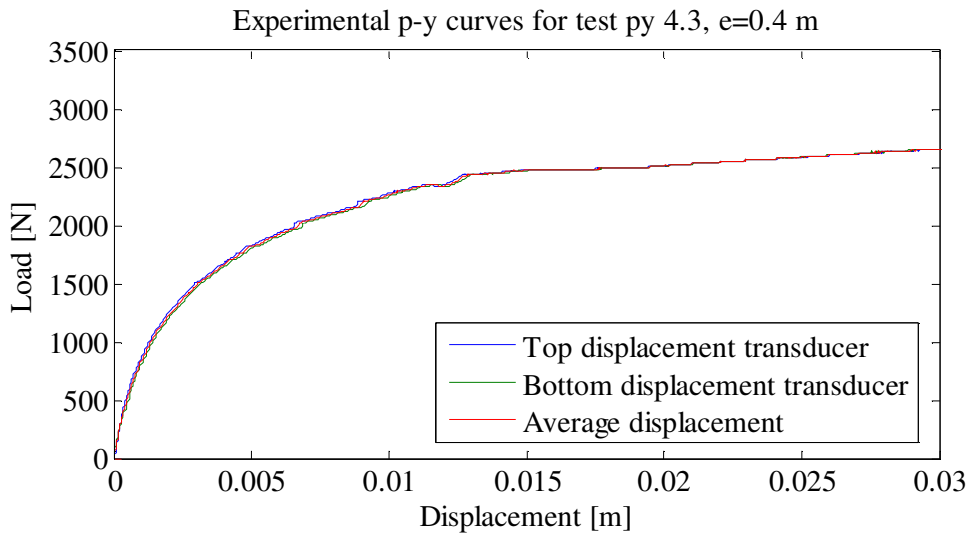

Figure C.12: Load-displacement curves for p-y experiment py 4.3 with e = 0.4 m.

D. Fit to experimental p-y curves

D.1 Fitted p-y curves

From the results of the p-y experiments three load-displacement curves for each overburden pressure is determined. The average of these three curves is the curve which is used in the non-linear Winkler model. In order to use the curves in the Winkler model, functions need to be fitted to the curves. The fitted functions consist of an initial linear part and a number of exponential functions. The fitted curves are shown in Figure D.1 to Figure D.20.

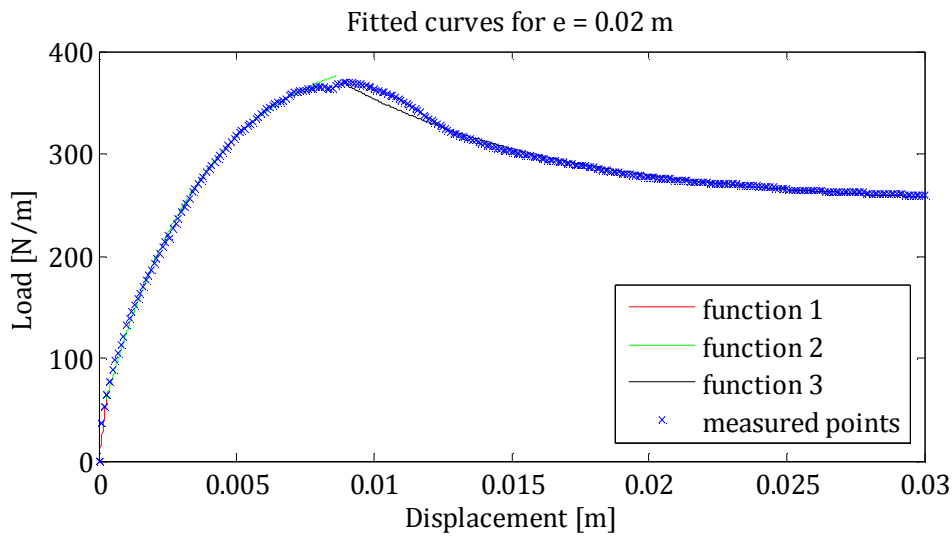

Figure D.1: Fitted curves for e = 0.02 m.

The expressions for the functions in Figure D.1 are:

$$F = \begin{cases} 216145 \cdot x & for\ 0 < x < 0.00027798 \\ 410.02 - 378.16 \cdot e^{-278.95 \cdot x} & for\ 0.00027798 < x < 0.00852668 \\ 249.04 + 365.14 \cdot e^{-124.85 \cdot x} & for\ 0.00852668 < x < 0.03 \end{cases}$$

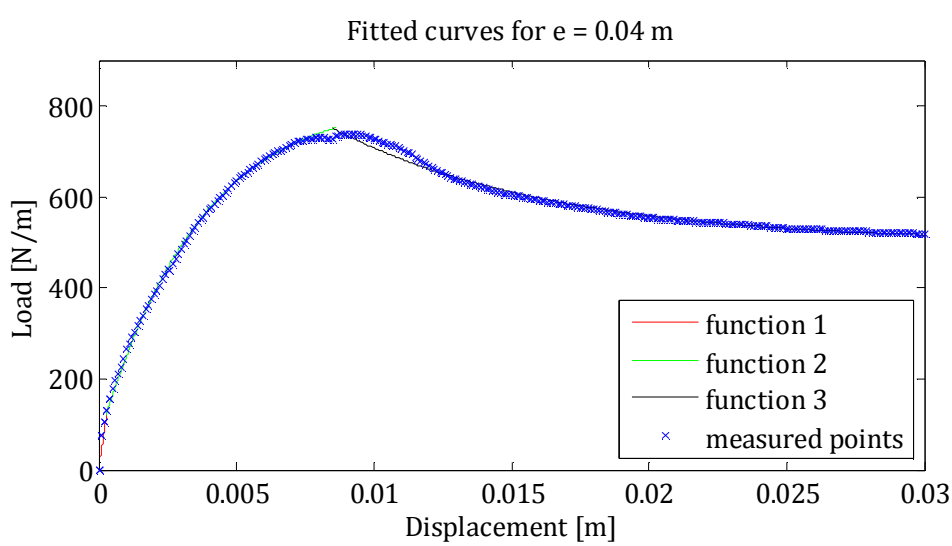

Figure D.2: Fitted curves for e = 0.04 m.

The expressions for the functions in Figure D.2 are:

$$F = \begin{cases} 432290 \cdot x & for\ 0 < x < 0.000277976 \\ 820.05 - 756.31 \cdot e^{-278.95 \cdot x} & for\ 0.000277976 < x < 0.00852668 \\ 498.08 + 730.27 \cdot e^{-124.85 \cdot x} & for\ 0.00852668 < x < 0.03 \end{cases}$$

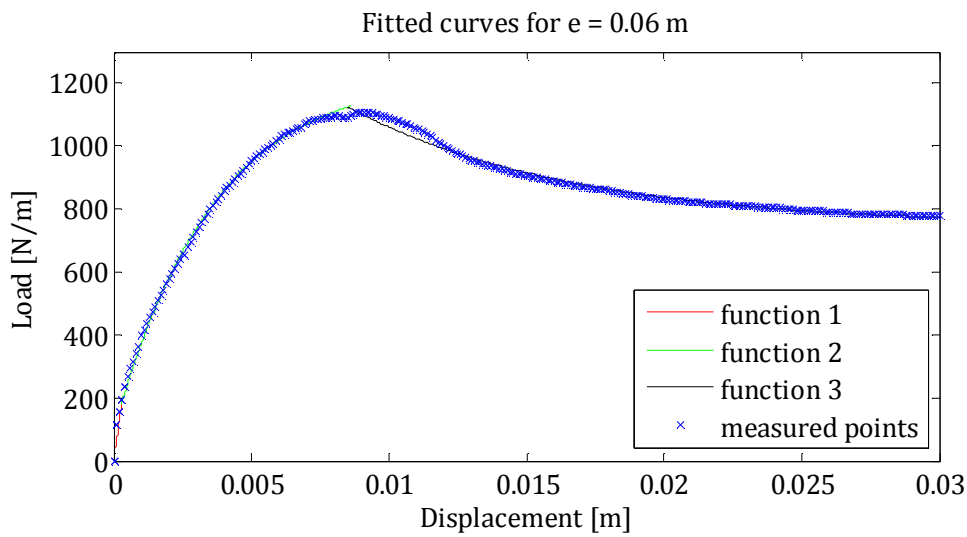

Figure D.3: Fitted curves for e = 0.06 m.

The expressions for the functions in Figure D.3 are:

$$F = \begin{cases} 648435 \cdot x & for\ 0 < x < 0.000277976 \\ 1230.08 - 1134.47 \cdot e^{-278.95 \cdot x} & for\ 0.000277976 < x < 0.00852668 \\ 747.12 + 1095.41 \cdot e^{-124.85 \cdot x} & for\ 0.00852668 < x < 0.03 \end{cases}$$

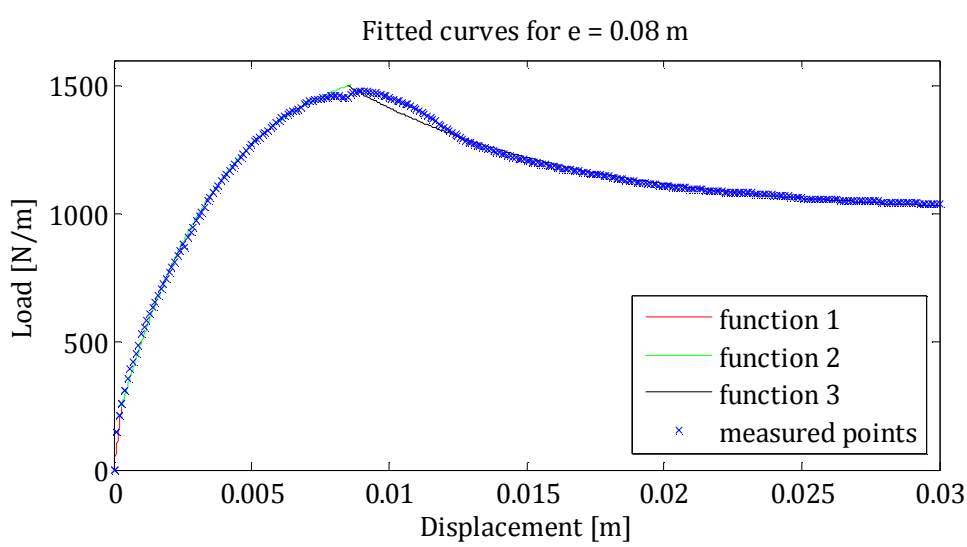

Figure D.4: Fitted curves for e = 0.08 m.

The expressions for the functions in Figure D.4 are:

$$F = \begin{cases} 864580 \cdot x & for\ 0 < x < 0.000277976 \\ 1640.1 - 1512.62 \cdot e^{-278.95 \cdot x} & for\ 0.000277976 < x < 0.00852668 \\ 996.16 + 1460.55 \cdot e^{-124.85 \cdot x} & for\ 0.00852668 < x < 0.03 \end{cases}$$

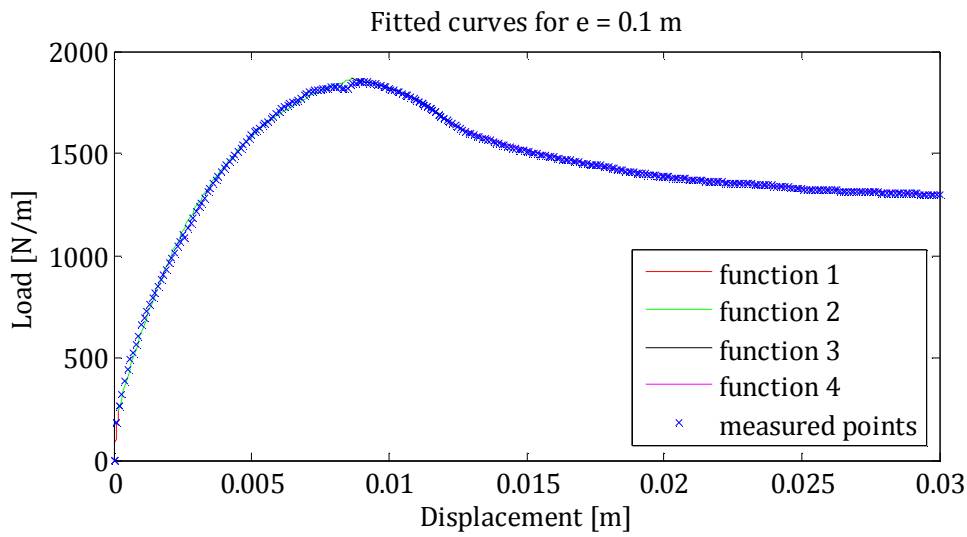

Figure D.5: Fitted curves for the average curve for the p-y experiments with e = 0.1 m.

The expressions for the functions in Figure D.5 are:

$$p(y) = \begin{cases} 1.449996 \cdot 10^{6} \cdot y & for\ 0 < y < 0.0001653 \\ 2009.13 - 1857.36 \cdot e^{-293.8 \cdot y} & for\ 0.0001653 \leq y < 0.008658 \\ 1907.95 - 0.60 \cdot e^{497.9 \cdot y} & for\ 0.008658 \leq y < 0.01224 \\ 1278.66 + 2315.60 \cdot e^{-150.4 \cdot y} & for\ 0.001224 \leq y \end{cases}$$

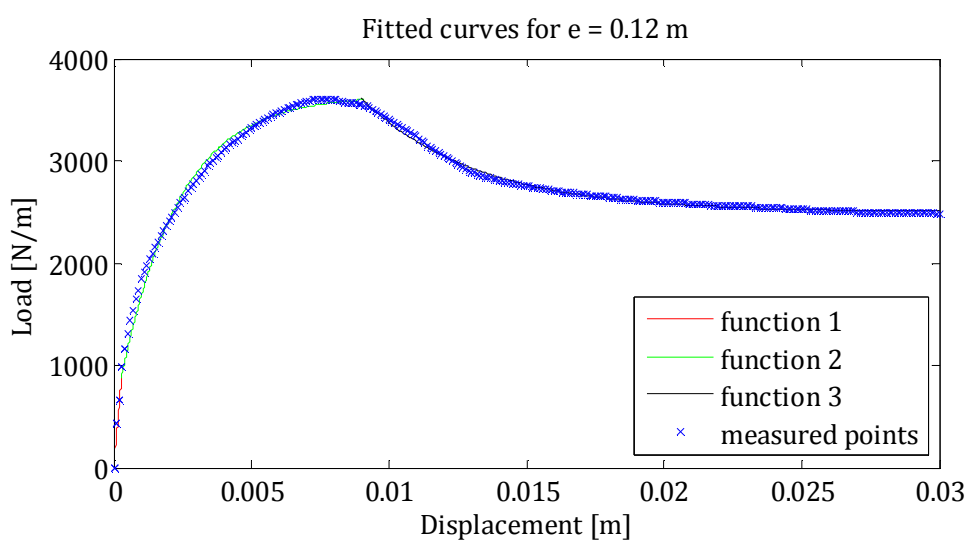

Figure D.6: Fitted curves for e = 0.12 m.

The expressions for the functions in Figure D.6 are:

$$F = \begin{cases} 3.11747 \cdot 10^6 \cdot x & for\ 0 < x < 0.00028781 \\ 3640.73 - 3144.0 \cdot e^{-473.46 \cdot x} & for\ 0.00028781 < x < 0.0090677 \\ 2500.88 + 9451.96 \cdot e^{-237.52 \cdot x} & for\ 0.0090677 < x < 0.03 \end{cases}$$

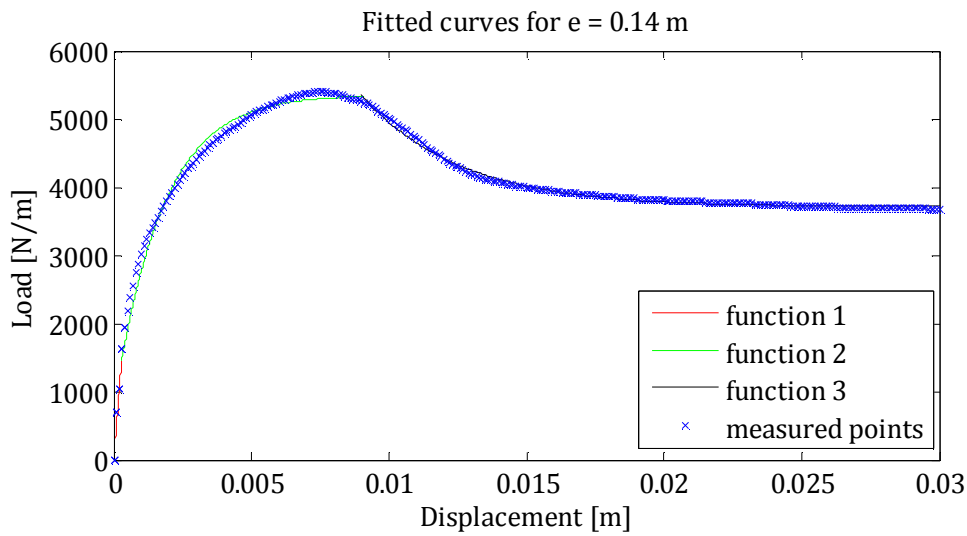

Figure D.7: Fitted curves for e = 0.14 m.

The expressions for the functions in Figure D.7 are:

$$F = \begin{cases} 5.15422 \cdot 10^6 \cdot x & for\ 0 < x < 0.00028097 \\ 5359 - 4594.55 \cdot e^{-573.12 \cdot x} & for\ 0.00028097 < x < 0.0090476 \\ 3705.62 + 20052.5 \cdot e^{-277.53 \cdot x} & for\ 0.0090476 < x < 0.03 \end{cases}$$

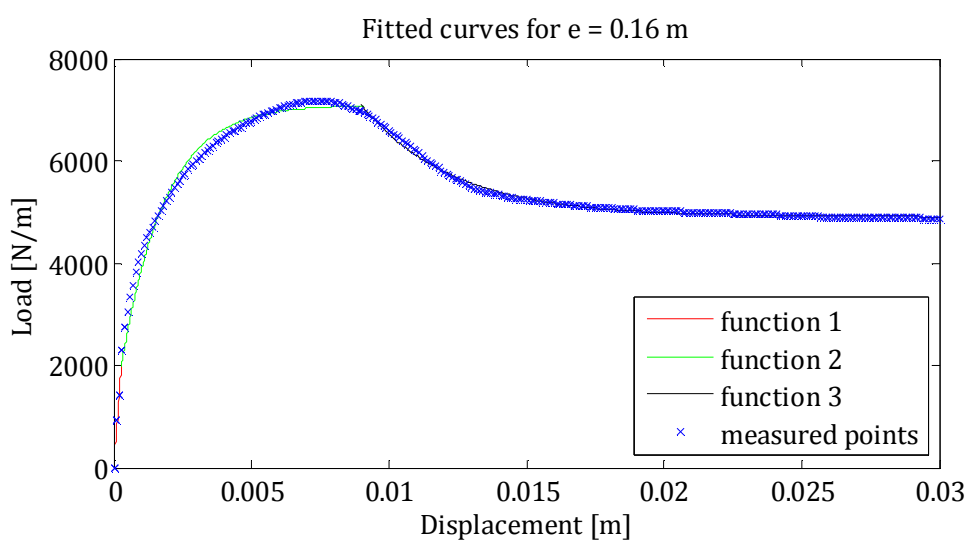

Figure D.8: Fitted curves for e = 0.16 m.

The expressions for the functions in Figure D.8 are:

$$F = \begin{cases} 7.19097 \cdot 10^6 \cdot x & for\ 0 < x < 0.000275698 \\ 7096.58 - 6092.88 \cdot e^{-635.24 \cdot x} & for\ 0.000275698 < x < 0.009034 \\ 4905.67 + 32743.86 \cdot e^{-300.35 \cdot x} & for\ 0.009034 < x < 0.03 \end{cases}$$

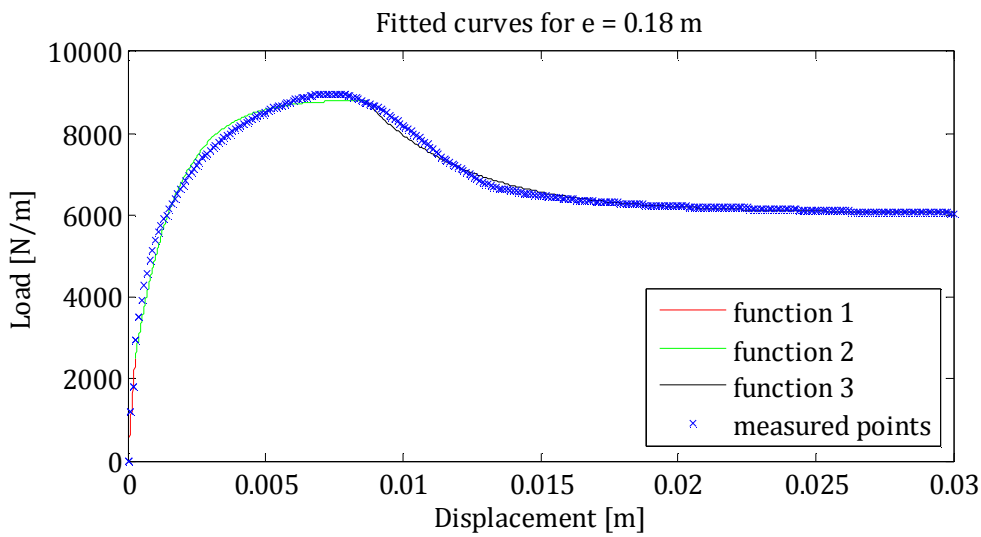

Figure D.9: Fitted curves for e = 0.18 m.

The expressions for the functions in Figure D.9 are:

$$F = \begin{cases} 9.2277 \cdot 10^6 \cdot x & for\ 0 < x < 0.000272014 \\ 8839.7 - 7610.74 \cdot e^{-677.62 \cdot x} & for\ 0.000272014 < x < 0.0086085 \\ 6064.88 + 26605.99 \cdot e^{-263.53 \cdot x} & for\ 0.0086085 < x < 0.03 \end{cases}$$

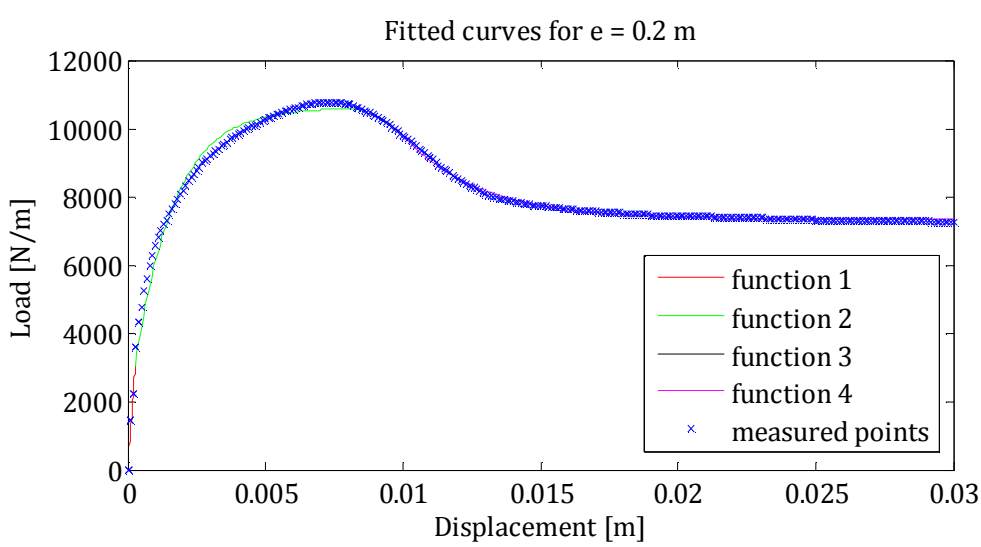

Figure D.10: Fitted curves for the average curve for the p-y experiments with e = 0.2 m.

The expressions for the functions in Figure D.10 are:

$$p(y) = \begin{cases} 1.128803 \cdot 10^7 \cdot y & for\ 0 < y < 0.000269 \\ 10600.83 - 9142.08 \cdot e^{-706.11 \cdot y} & for\ 0.000269 \leq y < 0.008462 \\ 11965.64 - 127.31 \cdot e^{282.3 \cdot y} & for\ 0.008462 \leq y < 0.009899 \\ 7327.80 + 88193.63 \cdot e^{-357.7 \cdot y} & for\ 0.009899 \leq y \end{cases}$$

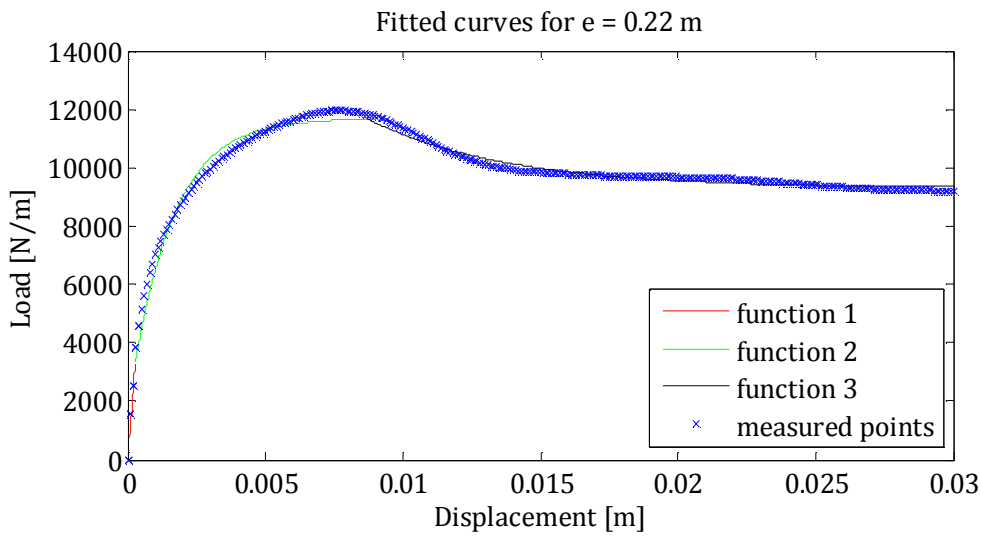

Figure D.11: Fitted curves for e = 0.22 m.

The expressions for the functions in Figure D.11 are:

$$F = \begin{cases} 1.21962 \cdot 10^7 \cdot x & for\ 0 < x < 0.00027192 \\ 11684.99 - 10010.20 \cdot e^{-658.7 \cdot x} & for\ 0.00027192 < x < 0.008761 \\ 9299.53 + 13543.24 \cdot e^{-199.75 \cdot x} & for\ 0.008761 < x < 0.03 \end{cases}$$

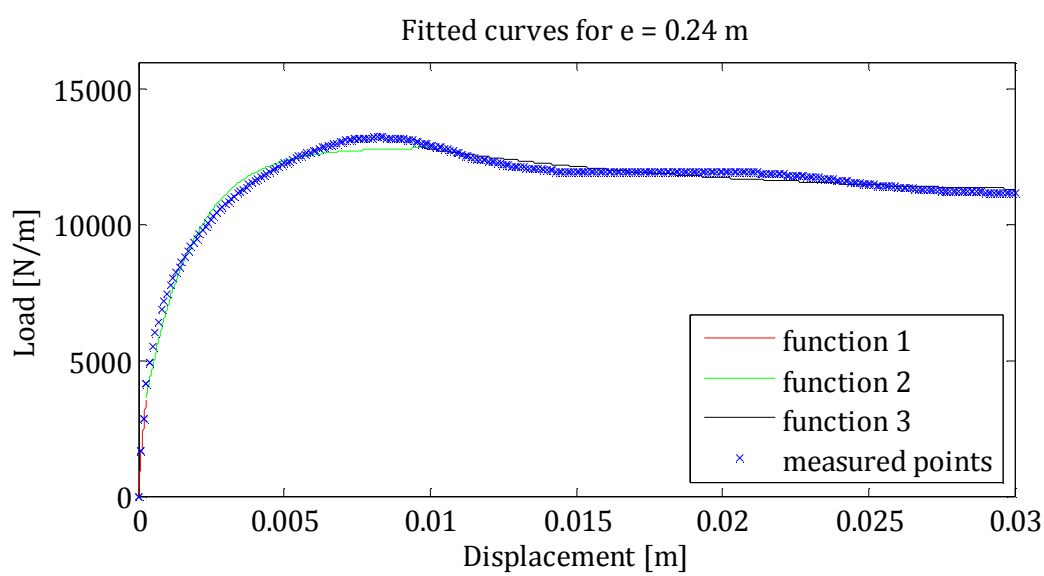

Figure D.12: Fitted curves for e = 0.24 m.

The expressions for the functions in Figure D.12 are:

$$F = \begin{cases} 1.31278 \cdot 10^7 \cdot x & for\ 0 < x < 0.0002757 \\ 12848.41 - 10918.66 \cdot e^{-609.78 \cdot x} & for\ 0.0002757 < x < 0.0098187 \\ 11037.45 + 4456.1 \cdot e^{-93.26 \cdot x} & for\ 0.0098187 < x < 0.03 \end{cases}$$

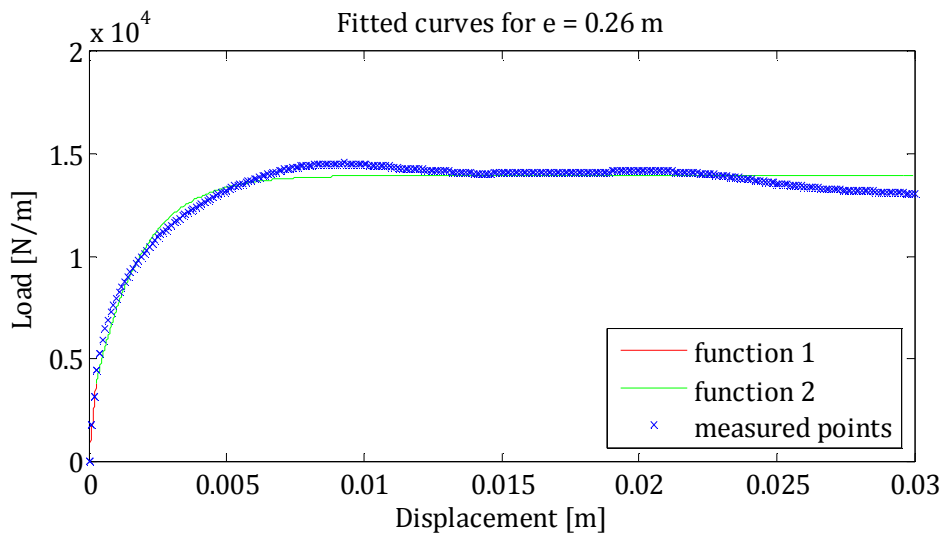

Figure D.13: Fitted curves for e = 0.26 m.

The expressions for the functions in Figure D.13 are:

$$F = \begin{cases} 1.40595 \cdot 10^7 \cdot x & for\ 0 < x < 0.00026907 \\ 13963.26 - 11947.92 \cdot e^{-595.05 \cdot x} & for\ 0.00026907 < x < 0.03 \end{cases}$$

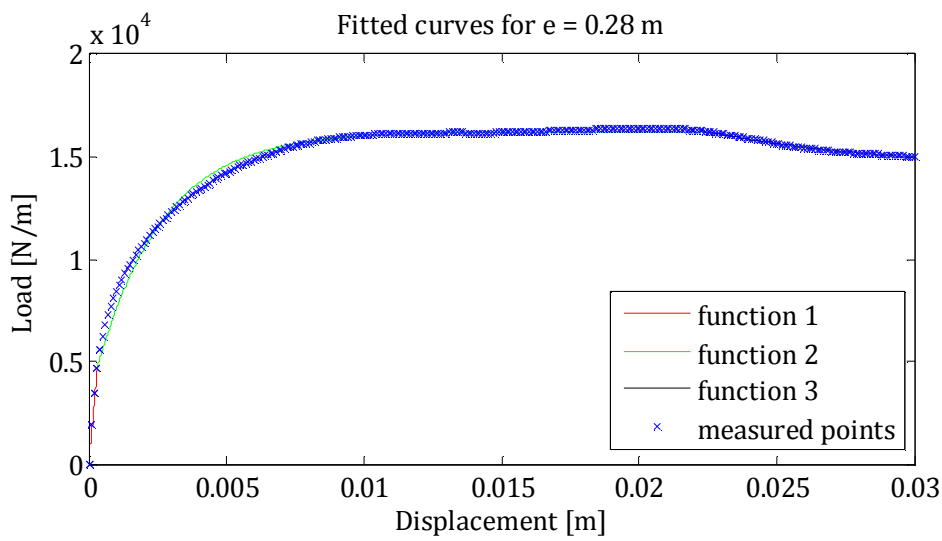

Figure D.14: Fitted curves for e = 0.28 m.

The expressions for the functions in Figure D.14 are:

$$F = \begin{cases} 1.49912 \cdot 10^7 \cdot x & for\ 0 < x < 0.00031834 \\ 16241.89 - 13069.36 \cdot e^{-410.15 \cdot x} & for\ 0.00031834 < x < 0.022485 \\ 14400.14 + 58076.55 \cdot e^{-153.51 \cdot x} & for\ 0.022485 < x < 0.03 \end{cases}$$

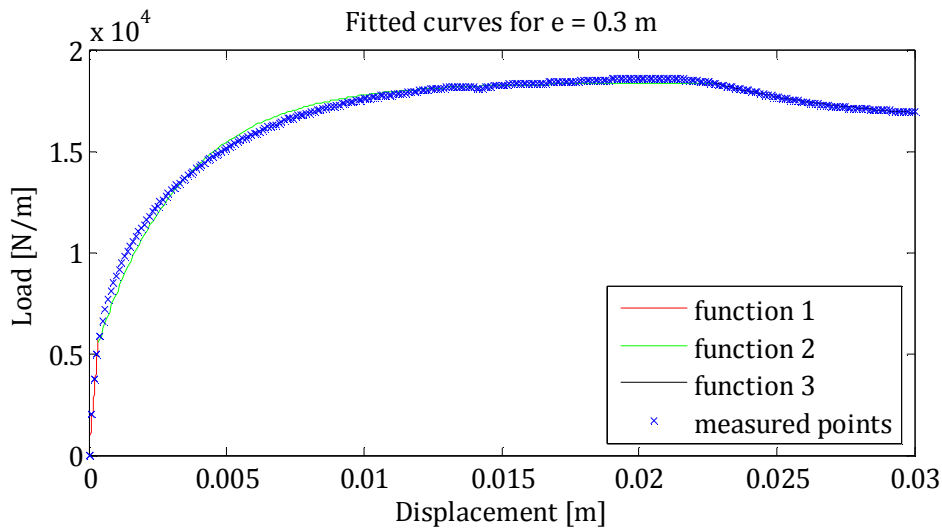

Figure D.15: Fitted curves for the average curve for the p-y experiments with e = 0.3 m.

The expressions for the functions in Figure D.15 are:

$$p(y) = \begin{cases} 1.15958 \cdot 10^7 \cdot y & for\ 0 < y < 0.0003508 \\ 18423.41 - 14335.99 \cdot e^{-319.73 \cdot y} & for\ 0.0003508 \leq y < 0.02280 \\ 16438.46 + 149378.92 \cdot e^{-189.78 \cdot y} & for\ 0.02280 \leq y \end{cases}$$

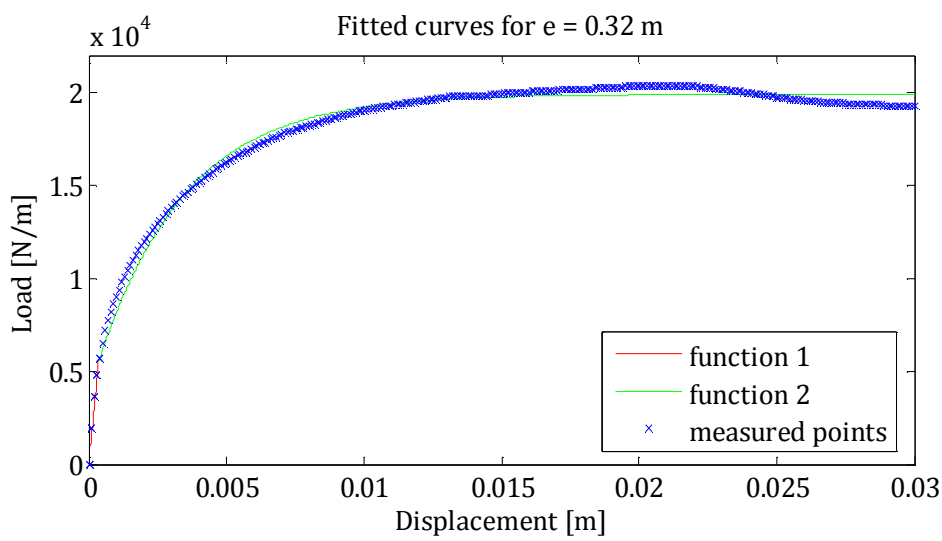

Figure D.16: Fitted curves for e = 0.32 m.

The expressions for the functions in Figure D.16 are:

$$F = \begin{cases} 1.54521 \cdot 10^7 \cdot x & for\ 0 < x < 0.000356496 \\ 19887.59 - 16084.25 \cdot e^{-314.38 \cdot x} & for\ 0.000356496 < x < 0.0031 \end{cases}$$

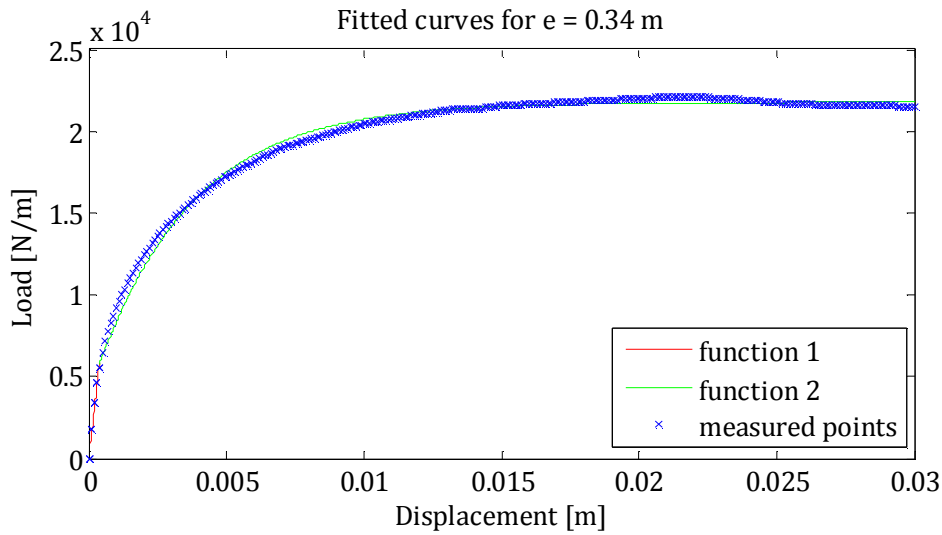

Figure D.17: Fitted curves for e = 0.34 m.

The expressions for the functions in Figure D.17 are:

$$F = \begin{cases} 1.49814 \cdot 10^7 \cdot x & for\ 0 < x < 0.00038608 \\ 21760.97 - 17833.19 \cdot e^{-284.70 \cdot x} & for\ 0.00038608 < x < 0.03 \end{cases}$$

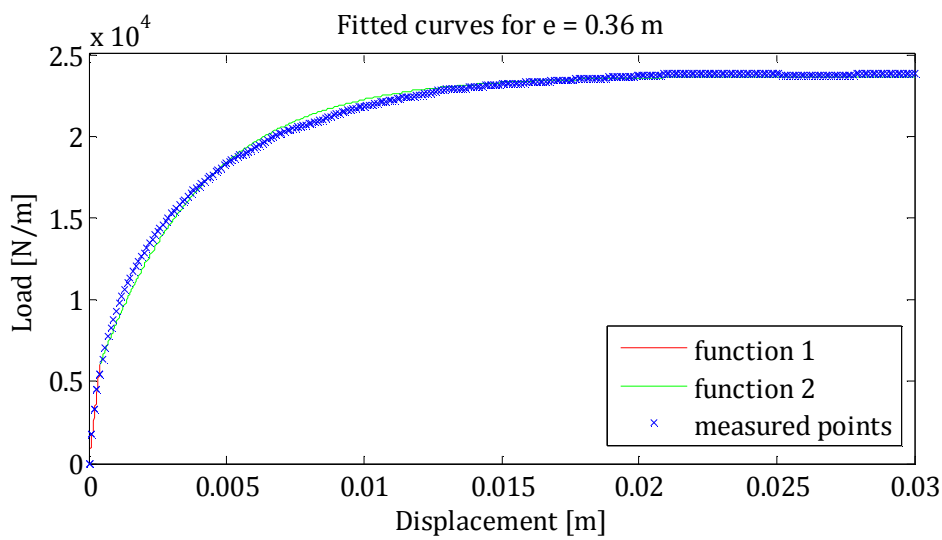

Figure D.18: Fitted curves for e = 0.36 m.

The expressions for the functions in Figure D.18 are:

$$F = \begin{cases} 1.45106 \cdot 10^7 \cdot x & for\ 0 < x < 0.00042015 \\ 23659.67 - 19605.16 \cdot e^{-261.80 \cdot x} & \end{cases}$$

$$for\ 0.00042015 < x < 0.03$$

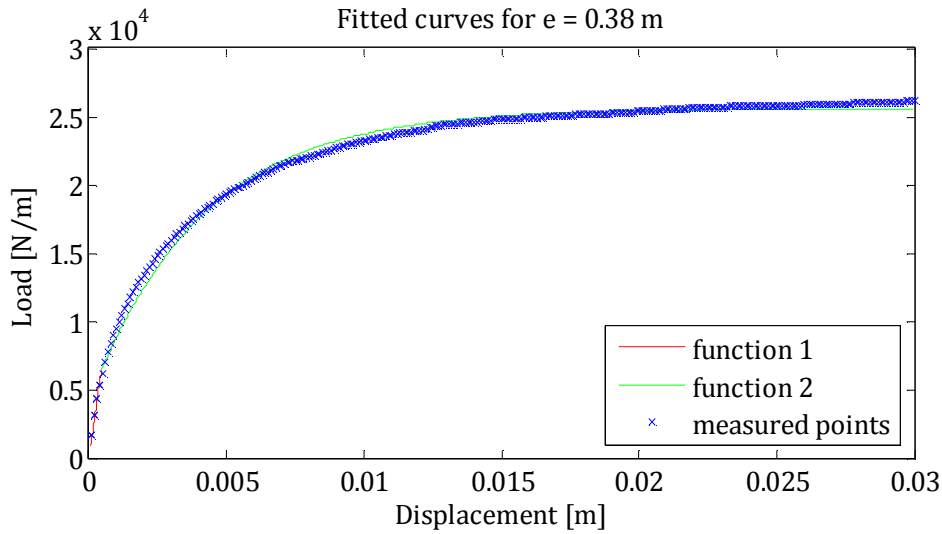

Figure D.19: Fitted curves for e = 0.38 m.

The expressions for the functions in Figure D.19 are:

$$F = \begin{cases} 1.40398 \cdot 10^7 \cdot x & for\ 0 < x < 0.00045943 \\ 25581.45 - 21396.56 \cdot e^{-243.59 \cdot x} & for\ 0.00045943 < x < 0.03 \end{cases}$$

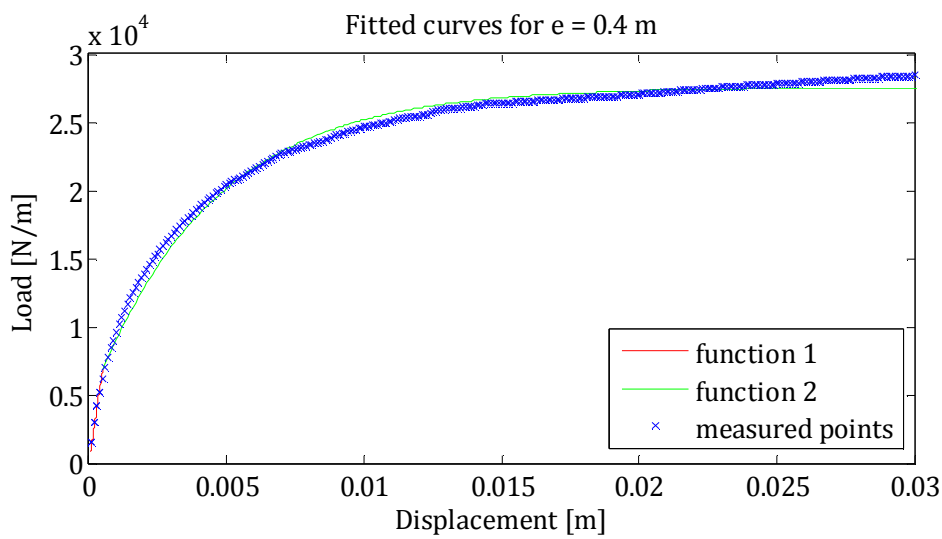

Figure D.20: Fitted curves for the average curve for the p-y experiments with e = 0.4 m.

The expressions for the functions in Figure D.20 are:

$$p(y) = \begin{cases} 1.36163 \cdot 10^7 \cdot y & for\ 0 < y < 0.0005034 \\ 27538.15 - 23206.81 \cdot e^{-228.79 \cdot y} & for\ 0.0005034 \leq y \end{cases}$$

E. Adjustment of static curves

In connection with the cyclic tests the pile has a tendency to move vertically upward or downward from its initial position. In order not to destroy the soil condition between the cyclic and the corresponding static test the pile cannot be moved. This entails that the results of the static tests are not directly comparable.
In this appendix it is evaluated how the different foundation depths influence the bearing capacity of a static test and adjustment factors are estimated.

The estimate is made using the MATLAB code with the beam on nonlinear Winkler foundation, $BEAM_{NL}$. In the program the top and bottom nodes are moved in accordance with the position of the pile after a cyclic test.

The bearing capacity is determined from the different analysis. The reference value of bearing capacity is the one corresponding to a foundation depth of 0.400 m.

In Figure E.1 a plot is made showing the influence of change in foundation depths. The calculations are based on the experimental p-y curves applied to the $BEAM_{NL}$.

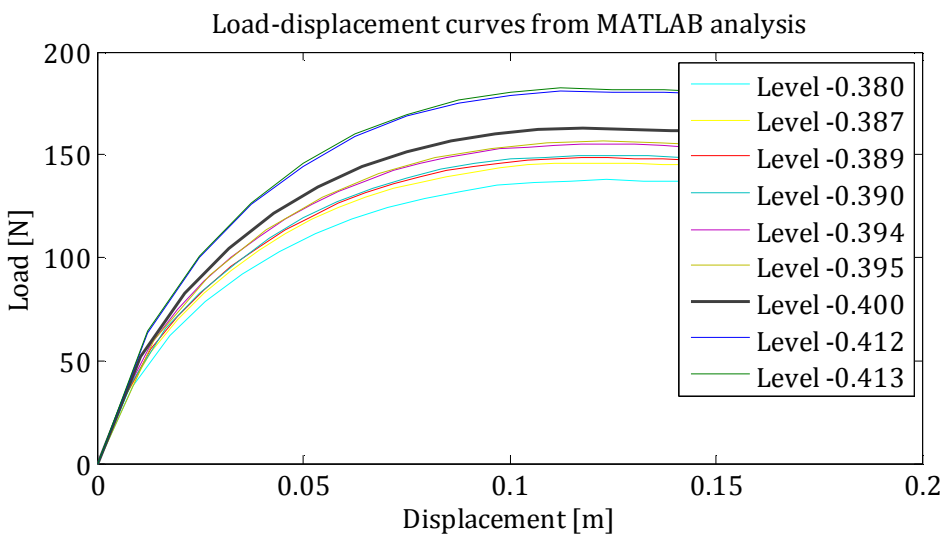

Figure E.1: Illustration of the influence of different foundation depths.

The different foundation depths and the corresponding adjustment factors are shown in Table E.1.

Foundation depth [m]	Bearing capacity [N]	Adjustment Factor
-0.380	137.65	1.1558
-0.387	146.26	1.1046
-0.389	148.82	1.0899
-0.390	149.63	1.0830
-0.394	155.14	1.0487
-0.395	156.44	1.0408
-0.400	163.17	1
-0.412	180.71	0.8910
-0.413	182.37	0.8823

Table E.1: Adjustment factors for different foundation depths.

F. Strain gauge test

F.1 Uncertainties in type and location of strain gauges

In this section the error in using single strain gauges instead of rosette gauges is examined. Also an examination of the effect of displacing the strain gauges by 5 mm from the centre of the pile is implemented.
In the examinations an Abaqus model of the pile is used. The pile is fixed in one end and loaded by a displacement load in the other end, see Figure F.1.

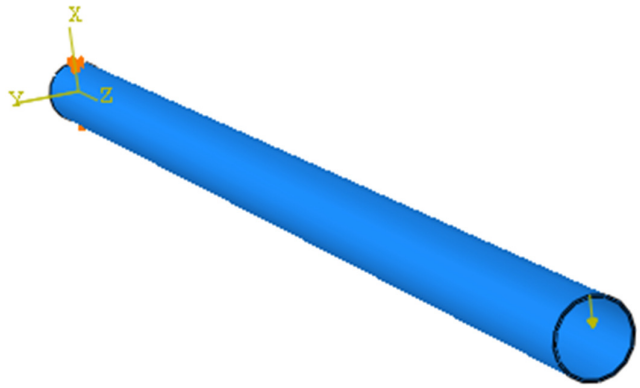

Figure F.1: Boundary conditions in the Abaqus model. The model is fixed in all direction at the orange marks and the yellow arrow illustrates the displacement load.

Figure F.2 shows the points where the stresses are read out. The points are named point 1, 2 and 3. The points next to these are displaced 5 mm from the centre.

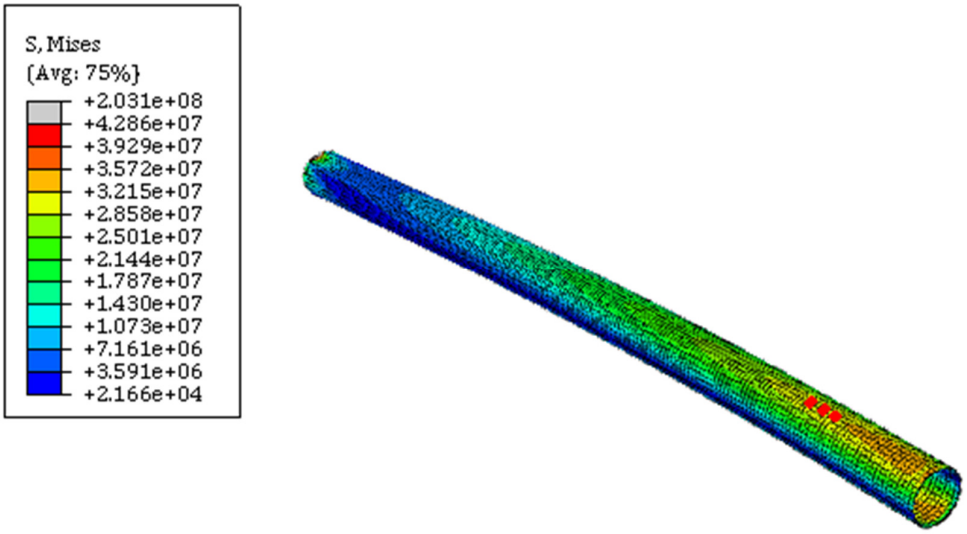

Figure F.2: Von Mises stresses in the Abaqus model and the reading points for the stresses. There are six points illustrated with red dots.

The strain component that the strain gauges measure corresponds to the component in the z-direction in the Abaqus model.

Table F-1 shows the Deviations in using single strain gauges instead of rosette gauges.
Table F-2 shows the deviations for displacing the strain gauges 5 mm from the centre of the pile.

Point	Von Mises stress [Mpa]	Stress component, σ_{33} [MPa]	Deviation [%]
1	31.9378	31.8802	0.18
2	31.4026	31.3459	0.18
3	30.8673	30.8115	0.18

Table F-1: Deviations between Von Mises stresses and the z-component of stress in the three points in the centre of the pile.

Table F-1 shows that the deviations of using single strain gauges instead of rosette gauges are very small and are assessed insignificant compared to other deviations in using strain gauges.

Punkt	ε_{33} in the centre line	ε_{33} displaced from the centre	Deviation [%]
1	-4.54032E-005	-4.54505E-005	0.004
2	-4.46419E-005	-4.46885E-005	0.1
3	-4.38807E-005	-4.39265E-005	0.1

Table F-2: Deviations between the stress in the z-direction at the centre of the pile and the point displaced 5 mm from the centre.

Table F-2 shows that the deviation if the strain gauges are displaced 5 mm from the centre is very small. The strain gauges are not displaced 5 mm when they are installed, but the pile can turn 5 mm during the test setup. The deviations are assessed negligible compared to other deviations when using strain gauges.

F.2 Examination of deviations

Three strain gauges are placed above the ground surface in order to examine the accuracy of the strain gauge measurements in each experiment. The moments calculated from the strain the these three strain gauges and theoretically calculated moments are shown in figure f.3 to figure f.5.

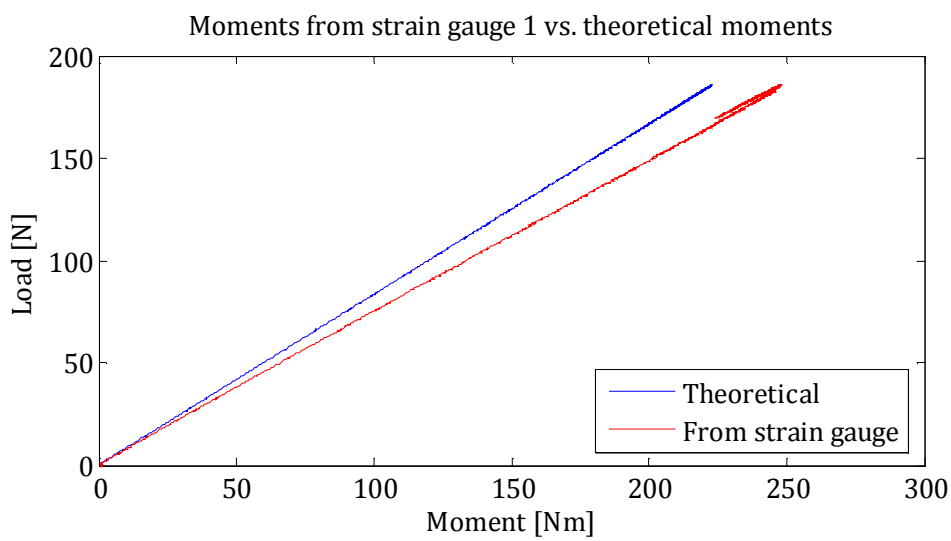

Figure F.3: Moments calculated from strain gauge 1 and theoretically calculated moments.

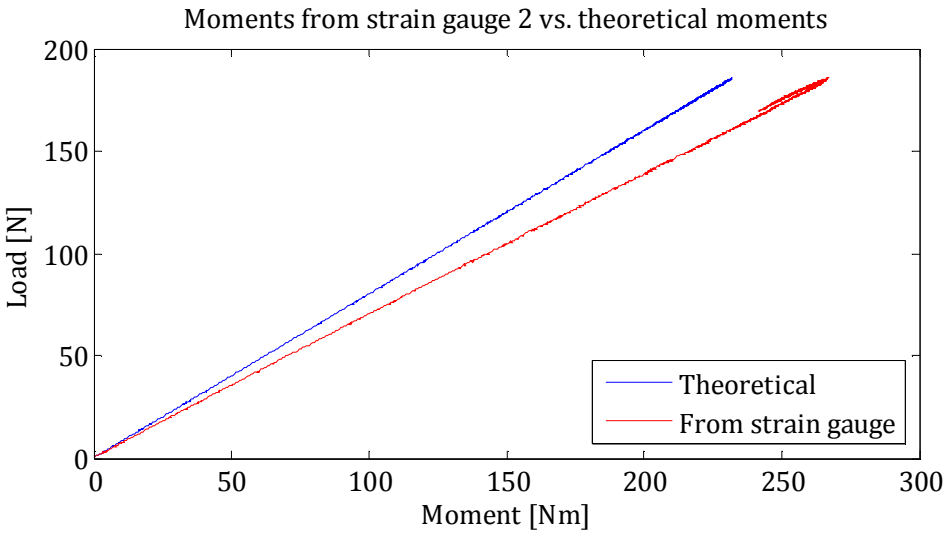

Figure F.4: Moments calculated from strain gauge 2 and theoretically calculated moments.

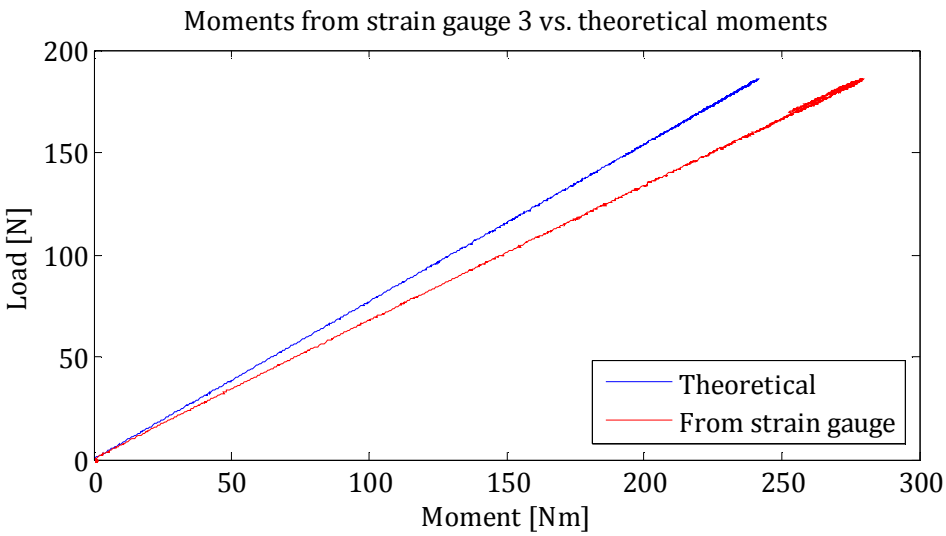

Figure F.5: Moments calculated from strain gauge 3 and theoretically calculated moments.

The figures show that the moments from the strain gauges deviate from the theoretically calculated moments. The deviations in percent with the force for the three strain gauges are shown in Figure F.6. Here it can be seen that for strain gauge 1 the deviations vary from 7 % for small loads up to 11 % for larger loads. The deviations vary between 10 and 14 % for strain gauge 2 and between 10 and 16 % for strain gauge 3.

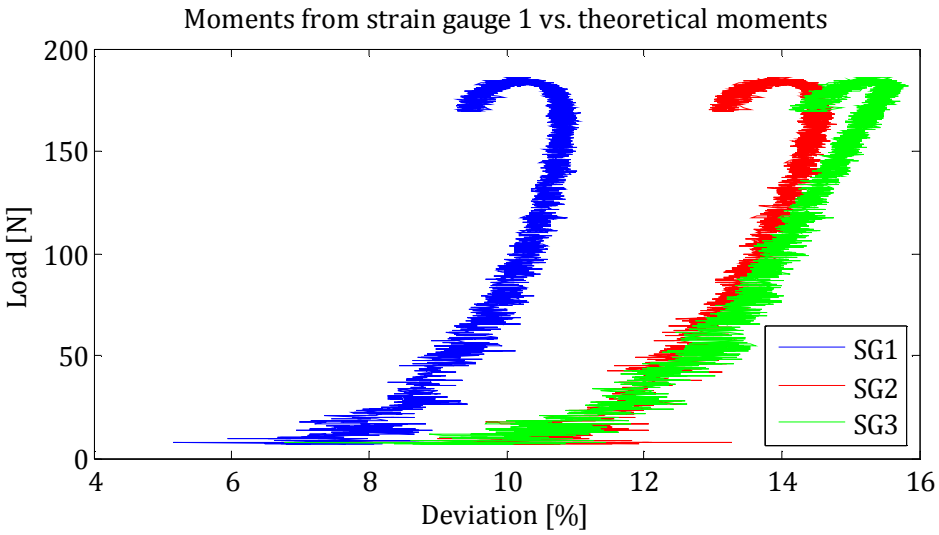

Figure F.6: Deviations in percent from the theoretical moments for the three strain gauges.

G. Sources of error

G.1 Calculation of force misalignment

The pile is loaded until the ultimate resistance of the sand. This means that the displacements at the top of the pile will be relatively large. Therefore the load will be applied misaligned from horizontal direction and the consequence of the misalignment is assessed in this section.
The box is placed so that the engine shaft has a distance to the pile of 2.0 m. This means that if the displacement at the top of the pile is 0.5 m at the ultimate load the system will look like illustrated in Figure G.1. It is assumed that the pile rotates 0.3 m below the ground surface.

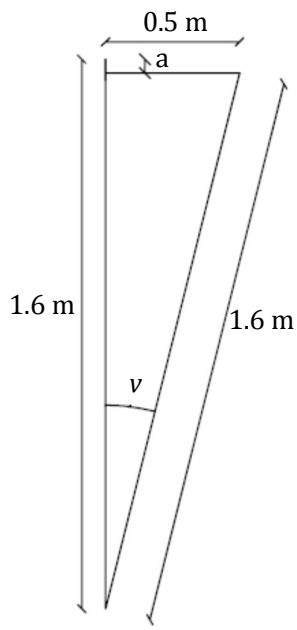

Figure G.1: Pile before and after being loaded to a displacement at the top of 0.5 m.

The angle, v, is determined:

$$v = tan^{-1}\left(\frac{0.5\ m}{1.6\ m}\right) = 17.6^{\circ} \tag{G.1}$$

From the angle the distance, a, that the pile top move downward is determined:

$$a = 1.6\ m - cos(17.6) \cdot 1.6\ m = 0.075\ m \tag{G.2}$$

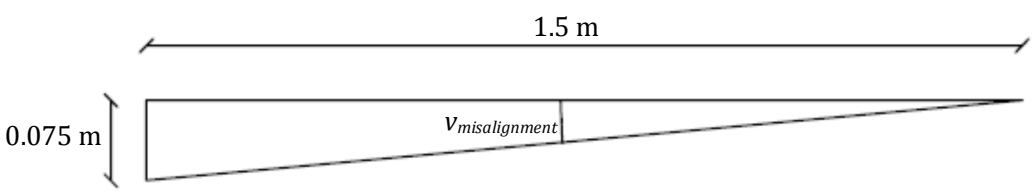

Figure G.2: Illustration of the misalignment of the force transducer.

The misalignment angle of the force, $v_{misalignment}$, is determined based on Figure G.2:

$$v_{misalignment} = tan^{-1}\left(\frac{0.075}{2.0\ m - 0.5\ m}\right) = 2.9^{\circ} \tag{G.3}$$

The load components are illustrated in

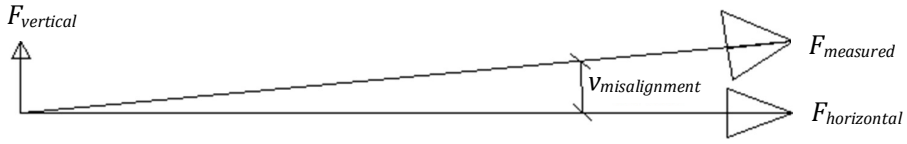

Figure G.3: Force components.

The horizontal force is determined as:

$$F_{horizontal} = cos(v_{misalignment}) \cdot F_{measured} \tag{G.4}$$

As $\cos(2.9^{\circ}) = 0.9987$ the horizontal component of the force equals 99.87 % of the measured force. Therefore the consequence of the load becoming misaligned is assessed to be negligible.

G.2 Inaccuracy in measuring displacements

The displacements at the pile top are measured using a wire displacement transducer. The end of the wire is attached to the pile top and the point of the displacement transducer is fixed. This means that the wire will have an oblique angle as the pile moves. The magnitude of this obliqueness at a horizontal displacement of the pile top of 0.5 m is assessed in this section. The system at a top displacement of the pile looks like in Figure G.4.

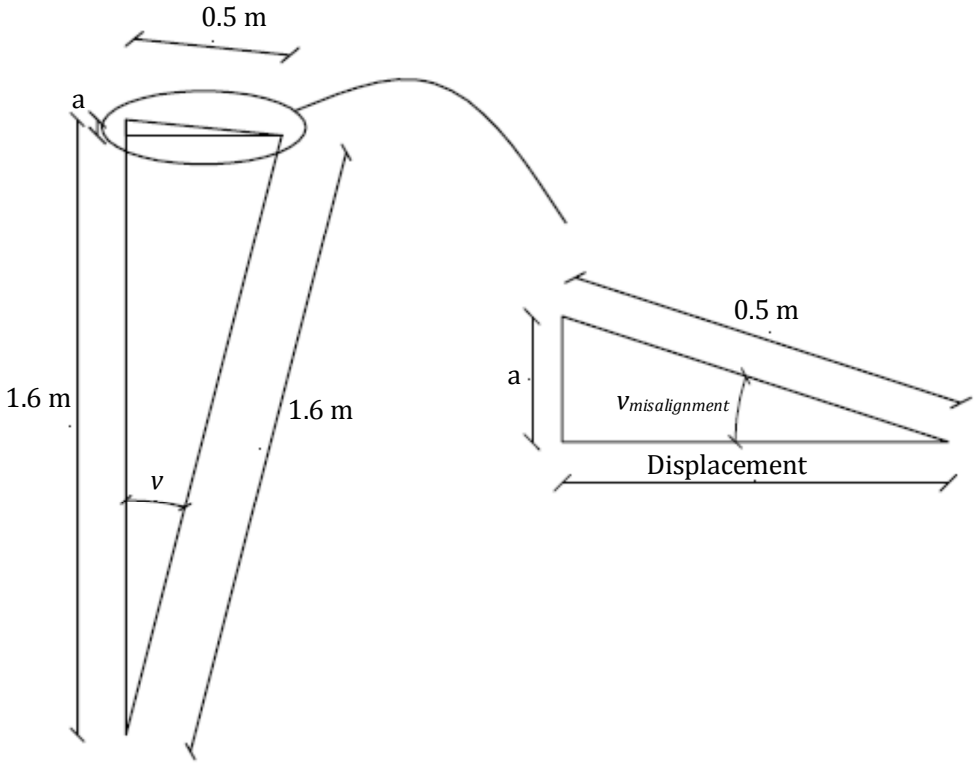

Figure G.4: Pile before and after being loaded to a displacement at the top of 0.5 m.

The angle, v, is determined:

$$v = tan^{-1}\left(\frac{0.5\ m}{1.6\ m}\right) = 17.6^{\circ} \tag{G.5}$$

From the angle the distance, a, that the pile top move downward is determined:

$$a = 1.6\ m - cos(17.6) \cdot 1.6\ m = 0.075\ m \tag{G.6}$$

The misalignment angle of the force, $v_{misalignment}$, is determined based on Figure G.2:

$$v_{misalignment} = sin^{-1}\left(\frac{0.075}{0.5\ m}\right) = 8.6^{\circ} \tag{G.7}$$

The actual horizontal displacement when the wire transducer measures a displacement of 0.5 m is determined as:

$$u_{horizontal} = \cos(8.6) \cdot 0.5\ m = 0.494\ m \tag{G.8}$$

The deviation between this displacement and the measured displacement is 1.2 % which is considered a negligible error compared to the accuracy of the wire transducer itself.

The displacements at the soil surface are measured with a laser displacement transducer. The laser measures the displacements at the same point above the ground surface during the entire experiment. This means that the point on the pile at which the laser point points to moves upward as the pile rotates. The extent of this error at a displacement of 0.1 m at the ground surface is determined in this section.
The displacement transducer is placed 0.141 m above the ground surface and the pile is assumed to rotate 0.3 m below the soil surface. The system at a displacement of 0.1 m is shown in Figure G.5

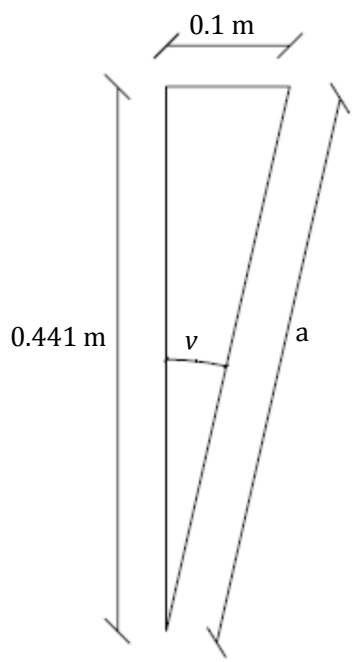

Figure G.5: Illustration of the point on the pile where the displacements are measured moving upward.

The angle, v, and the distance, a, a determined:
Højden af punktet på pælen som flytningerne måles i efter en flytning på 100 mm svarer til længden, a, der beregnes ud fra vinklen, v:

$$v = tan^{-1}\left(\frac{0.1\ m}{0.441\ m}\right) = 12.776^{\circ} \tag{G.9}$$

$$a = \frac{sin(12.776)}{0.1\ m} = 0.452\ m \tag{G.10}$$

This means that the point moves 0.012 m upward. The difference between the measured displacement and the displacement at the original point on the pile is determined. The difference in the displacement is illustrated in Figure G.6.

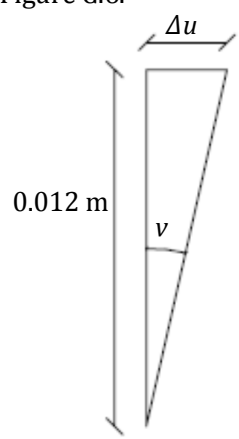

Figure G.6: u is the difference between the measured displacement and the displacement at the original point.

The difference between the measured displacement and the displacement at the original point, Δu, is determined as:

$$\Delta u = tan(12.776) \cdot 0.012\ m = 0.0027\ m \tag{G.11}$$

The deviation between the measured displacement and the displacement at the original point becomes:

$$\frac{(0.1\ m - 0.0027\ m) - 0.1\ m}{0.1\ m} \cdot 100\ \% = 2.7\ \% \tag{G.12}$$

This deviation is considered a negligible error compared to the accuracy of the wire transducer itself.

H. Determining displacements of the pile

The displacements in all points along the pile are determined using the programme, *piledisplacement* [CD/Programs/piledisplacement.m]. In this programme the displacements are determined using the strain gauge measurements and the measured displacements above the ground surface. Purpose is to determine the displacements of the pile below the ground surface, as this is not possible with ordinary displacement transducers. The programme also determines the moment distribution so that both the displacements and the moment distribution can be compared to the results of the finite element programmes.

The strain gauges measure strains in the pile below the ground surface. These strains can be converted into moments as plane stress is assumed. Besides the strains also displacements in two points above ground surface is measured during the static tests. When the moment distribution and two displacements are known, the displacements in all points along the pile can be determined.
Bernoulli-Euler beam theory gives an association between the moment distribution and the displacements. This is used in the programme, see equation (A.1):

$$\frac{M(z)}{EI} = \frac{d^2u(z)}{dz^2} \tag{H.1}$$

Where:

$M(z)$ is the moment distribution
$u(z)$ is the displacement perpendicular to the z-axis

The displacements are determined by integration of equation (A.1) twice. This produces two integration constants. These constants can be determined when measured displacements, u_1 and u_2 are known in the point z_1 and z_2.

The moment is determined in 9 points along the pile where strain gauges are installed. The moment above the ground surface is linearly distributed and the distribution below ground surface is unknown. The moment distribution below the ground surface can be estimated by fitting a function to the measuring points of the 7 strain gauges that are installed below the ground surface.
The moment distribution in the pile is described as two connected functions: An upper linear function, M_{upper}, which is valid above the ground surface, (z > 0) and a lower function, M_{lower}, which is valid below the ground surface.
To describe the moment distribution below the ground surface a polynomial is fitted to the data points from the strain gauges. A polynomial of 4th degree produces an eve curve with no fluctuation between the measuring points, see Figure H.1.

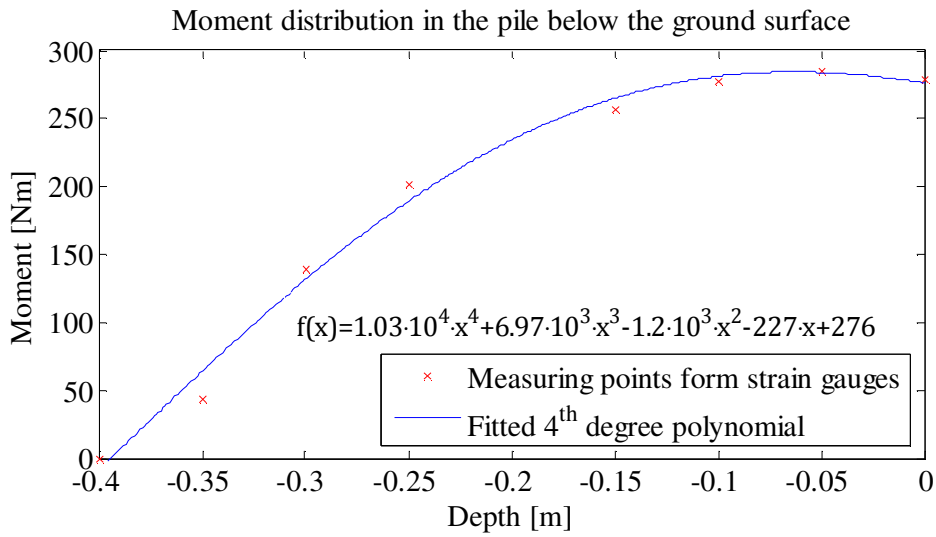

Figure H.1: Example of moment distribution in the pile below the ground surface using a 4th degree polynomial.

M_{lower} is therefore described as a polynomial of 4th degree:

$$M_{lower} = p_1 z^4 + p_2 z^3 + p_3 z^2 + p_4 z + p_5 \tag{H.2}$$

In order to insure continuity in the moment at the ground surface the function value $M_{new} = M_{lower}(0)$ is used to determine M_{upper}:

$$M_{upper} = \frac{-M_{new}}{L_A} \cdot z + M_{new} \tag{H.3}$$

Where L_A is the distance from the point of load application to the ground surface.
Both M_{upper} and M_{lower} are integrated twice. This results in two equations with two integration constants in each. The integration constants are called c_1 and c_2 in the upper equation, see equation H.4) and c_3 and c_4 in the lower equation, see equation
(H.5):

$$u(z)_{upper} = \int\int \frac{M_{upper}(z)}{EI} dzdz = \frac{1}{EI}\left(\frac{-M_{new}}{L_A \cdot 2 \cdot 3} z^3 + \frac{M_{new}}{2} z^2 + c_1 z + c_2\right) \tag{H.4}$$

$$u(z)_{lower} = \int\int \frac{M_{lower}(z)}{EI} dzdz = \frac{1}{EI}\left(\frac{p_1}{5 \cdot 6} z^6 + \frac{p_2}{4 \cdot 5} z^5 + \cdots + \frac{p_5}{2} z^2 + c_3 z + c_4\right) \tag{H.5}$$

The displacements are known in two points above the ground surface. This is used to determine the integration constants c_1 and c_2 by two equations with two unknown. There has to be continuity in the ground surface for both the displacements and the derived of the displacements. (angular displacement). Therefore $c_3 = c_1$ and $c_4 = c_2$.

The displacement figure corresponding to the moment distribution in Figure H.1 is shown in

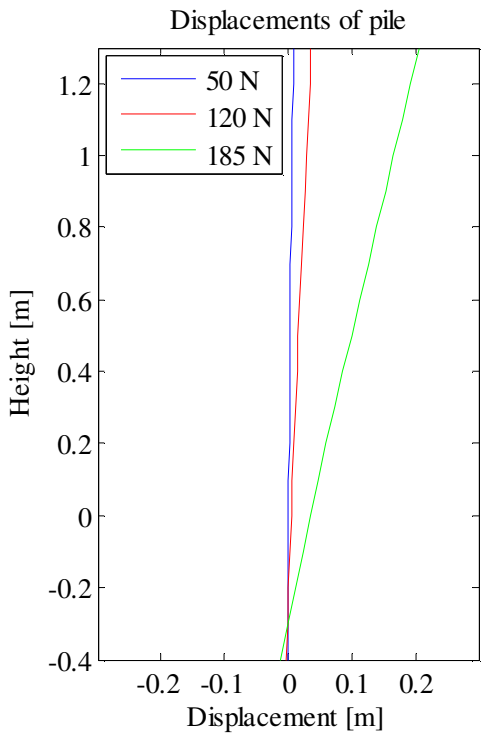

Figure H.2.

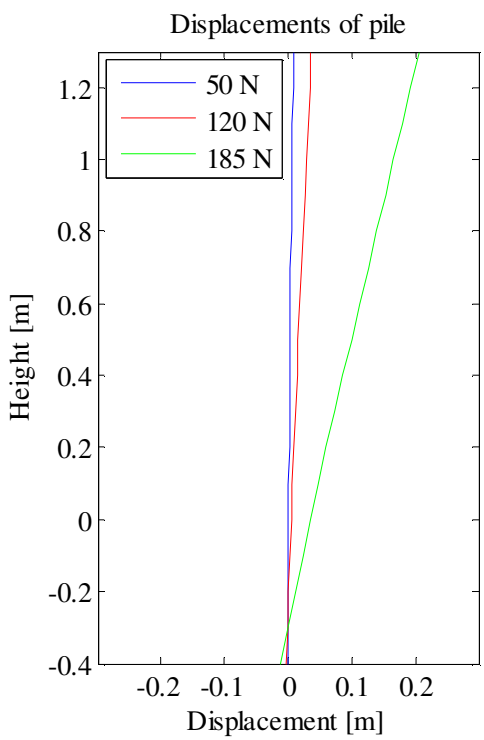

Figure H.2: The displacements in the pile at loads of 50 N, 120 N and 185 N. Results from static test s.0.2 has been used.

The figure shows that the pile is pushed into the soil at small loads and for the ultimate load the pile rotates. The movement of the pile is approximately rigid. The point of zero deflection is determined by finding the real solution for $u(z) = 0$.
The method used in the programme is assessed to be good. Uncertainty is related to fitting a polynomial to the strain gauge measurements in order to determine the moment variation, but as the polynomial fits very well to the data this I assessed as reasonable.
The programme can be used to determine the moment variation and the displacements. It cannot be used to determine the earth pressure below the soil surface as this will entail differentiating the moment distribution and for this a polynomial is not accurate enough.

I. Earth pressure from strain gauges

In the static experiments, eight strain gauges are placed below the ground surface with an internal distance of 0.005 m. One of the strain gauges is out of order during the experiments. Therefore there is only seven strain gauges to determine the moment distribution below the ground surface from. The moment distribution is determined by fitting a function to the moments determined from the strain gauges below the ground surface.
The fitted moment distributions with four different degrees of polynomials are shown in Figure I.1.

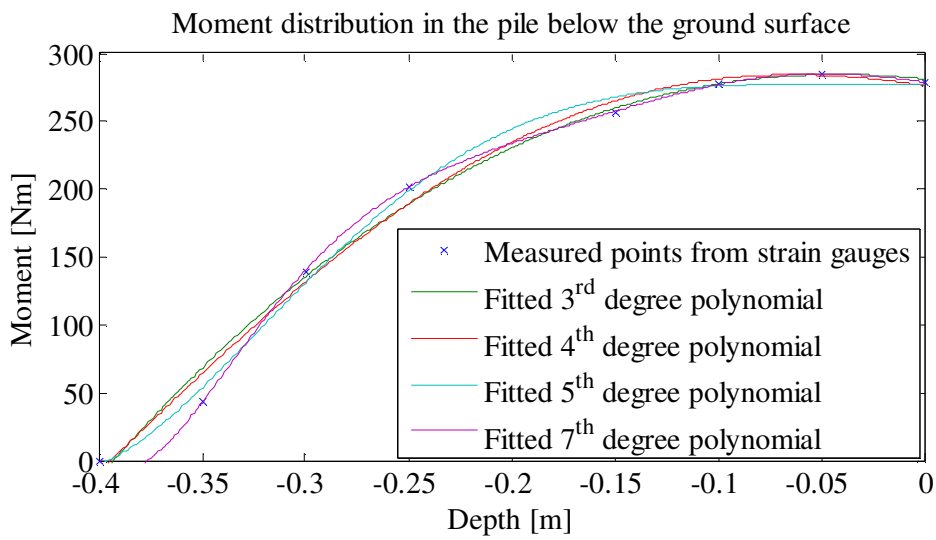

Figure I.1: Moment distribution below ground surface using four different degrees of polynomials.

Figure I.1 shows that the moment distribution is somewhat different depending on which polynomial is chosen. In order to determine the earth pressure from the moment curve, the curve must be integrated with respect to the depth, x:

$$V(x) = \frac{dM}{dx} \tag{I.1}$$

The integrated moment curves from Figure I.1 are shown in Figure I.2.

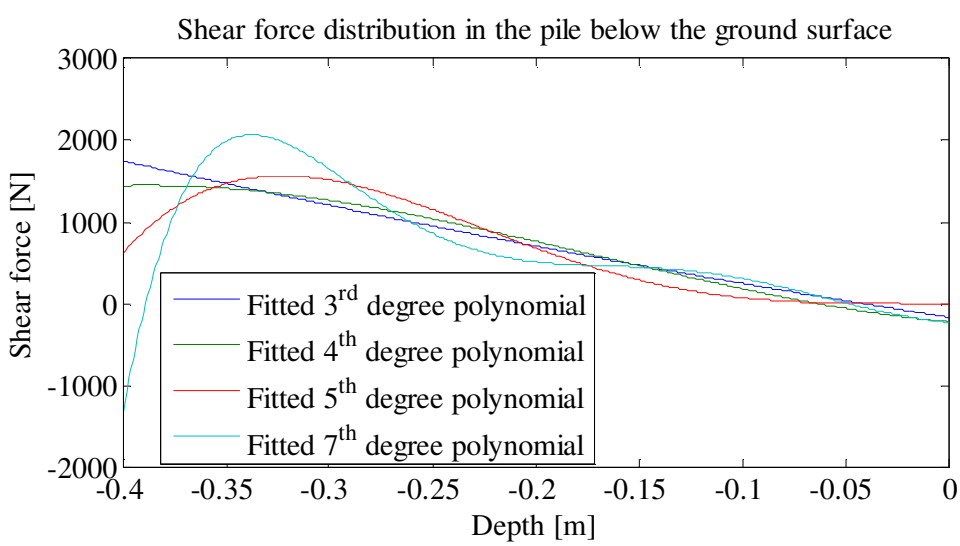

Figure I.2: Shear force distribution with four different degrees of polynomials.

Figure I.2 shows that even though the differences in the moment distributions in Figure I.1 are small, the distributions of the shear force are very different; especially towards the bottom og the pile.

The earth pressures are determined as the difference in shear force for each point below the ground surface, see Figure I.3.

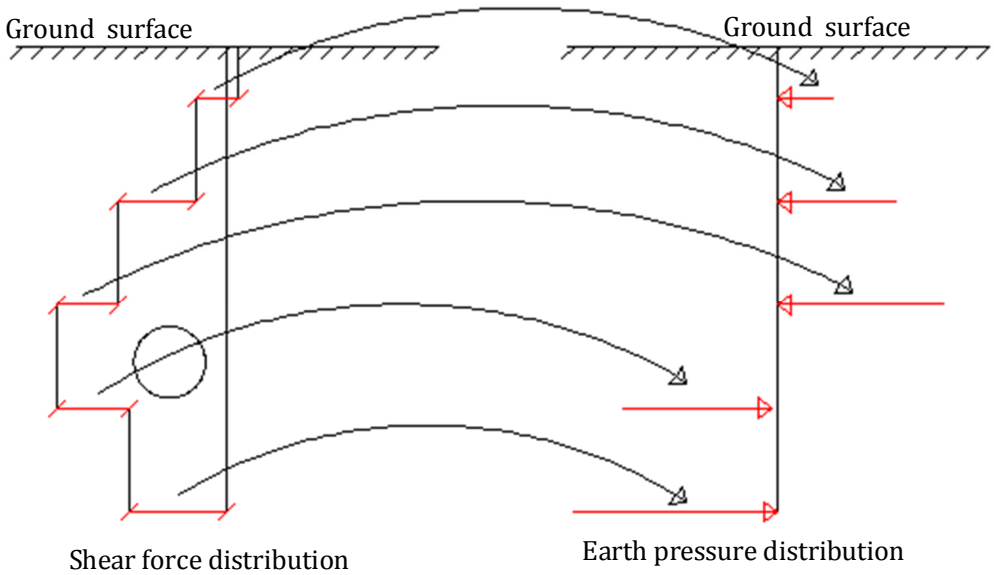

Figure I.3: Illustration of how the earth pressure is determined from the shear force distribution.

Figure I.4 shows the earth pressure distribution below the ground surface determined from the shear forces.

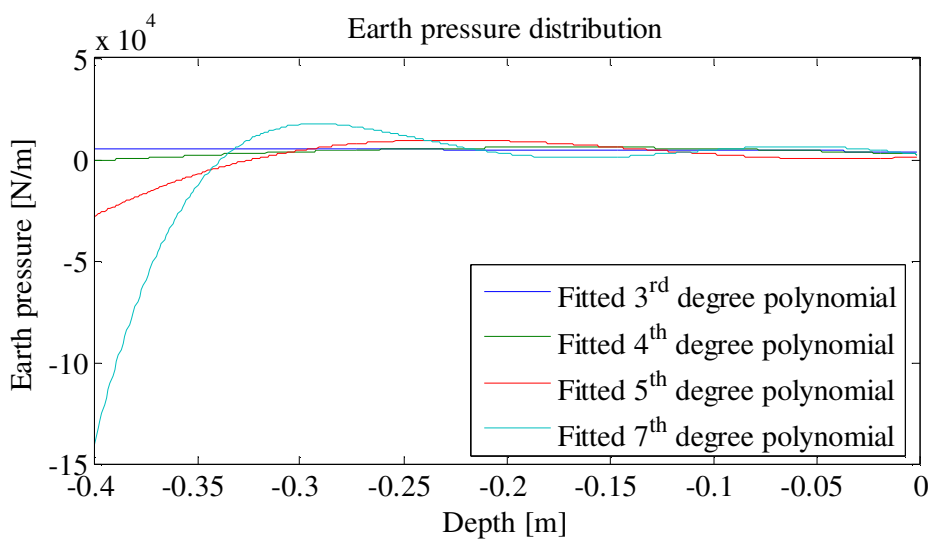

Figure I.4: Earth pressure distribution with four different degrees of polynomials.

In appendix H it is described how the displacements along the pile can be determined from the moment distribution. This is done by integration the distribution twice. Figure I.5 shows the moment distributions in Figure I.1 integrated once. It can be seen that integration of the moment distribution even though the polynomials are different, gives very similar curves.

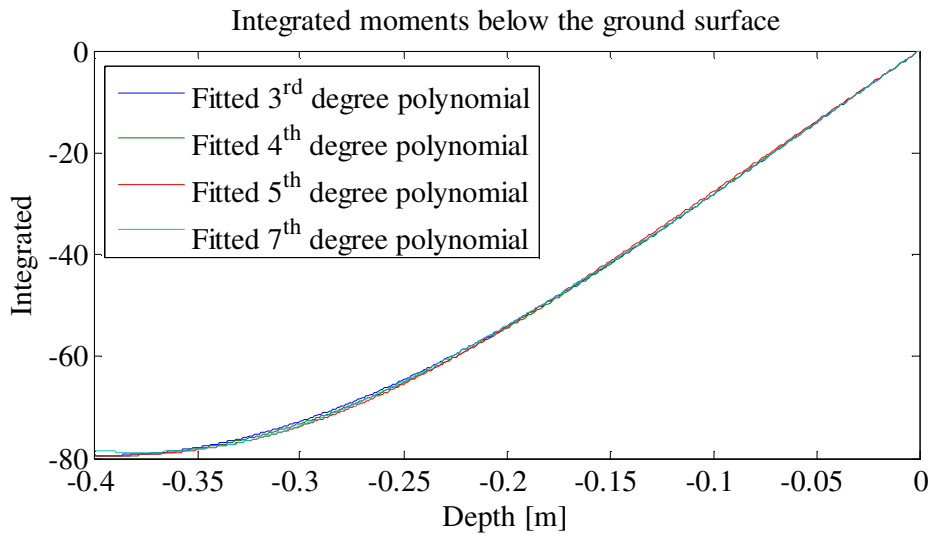

Figure I.5: Integrated moment distributions using four different degrees of polynomials.

On basis of this, it can be concluded that it is OK to integrate the moment curves as the result does not depend very much on which polynomial is chosen. But integrating of the moment curves requires very specific knowledge of the course of the moment curve, which cannot be attained with the amount of strain gauges on the pile.

J. Dimensioning of connecting rod

The connecting rod is mounted in a bearing that is fixed to the pulley. In the other end the connecting rod is assembled to the force measurer, which is attached to the pile through a bearing. The system is illustrated on Figure J.1.

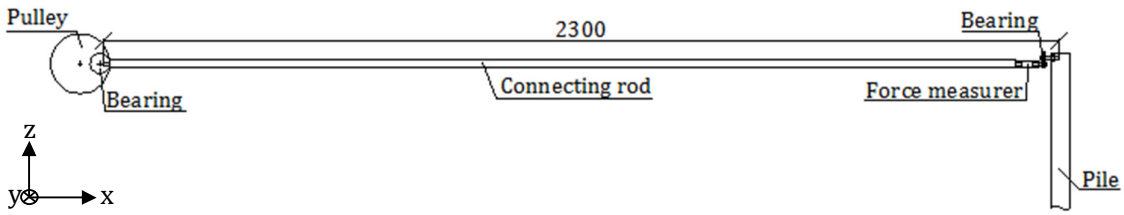

Figure J.1: Load application system used in connection with the displacement controlled cyclic pile experiments. Measure in mm.

From the static pile experiments it is known, that a force around 200 N will cause failure in the sand. The cyclic tests are not supposed to cause global failure, anyway the connecting rod is dimensioned for a force of that size.

The joint between the pile and the connecting rod leads to a certain eccentricity, see

Figure J.2. This causes a bending moment in the rod, which has to be taken into consideration when dimensioning the rod.

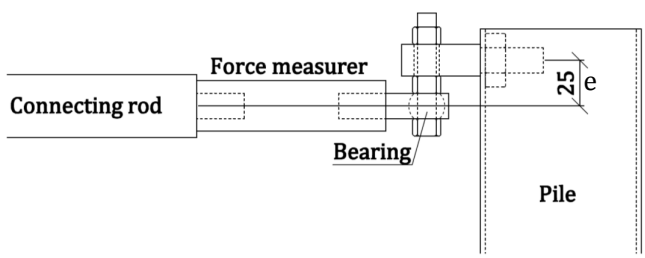

Figure J.2: Joint between connecting rod and pile. Measure in mm.

The bearing fixed to the pulley has a width on 17 mm. The width of the connecting rod therefore must not exceed 17 mm.

A standard tube profile is chosen for the connecting rod, a 20/15/1.5 mm steel profile from Sanistål, see Figure J.3.

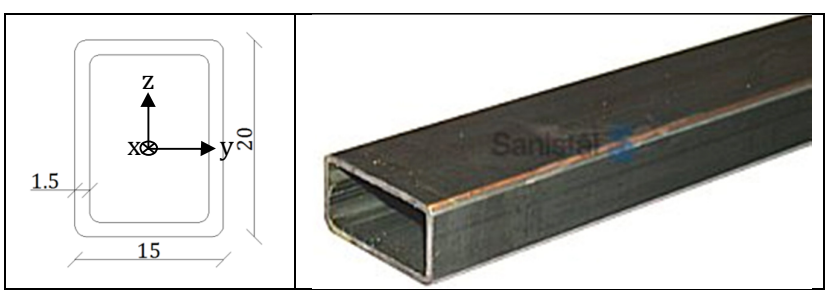

Figure J.3: Standard tube profile chosen for connecting rod. Measure in mm.

J.1 Profile data

The tube profile is made in accordance with DIN 2395 standard[1]. The relevant data appear from Table J.1.

Tube profile 20/15/1.5 mm								
$\boldsymbol{A}$ [m²]	$r\left[\frac{\mathrm{N}}{\mathrm{m}}\right]$	f_y [MPa]	I_y [m⁴]	I_x [m⁴]	i_y[m]	i_x [m]	W_y [m³]	W_{pl} [m³]
$\mathbf{9.6 \cdot 10^{-5}}$	7.365	235	$5.087 \cdot 10^{-9}$	$3.177 \cdot 10^{-9}$	0.0073	0.0058	$5.087 \cdot 10^{-7}$	$6.33 \cdot 10^{-7}$

Table J.1: Profile data, 20/15/1.5 mm.

J.2 Control of profile bearing capacity

The static system for the connecting rod is shown on Figure J.4. The uniformly distributed load represents the weight of the rod.

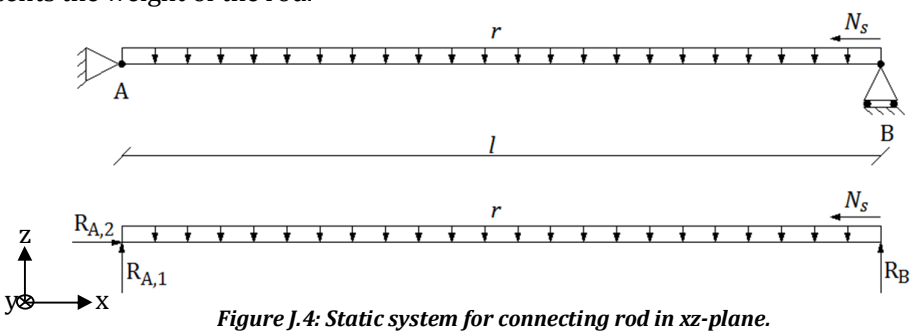

Figure J.4: Static system for connecting rod in xz-plane.

J.2.1 Calculation of section forces

Initially the section forces are calculated from the equilibrium equations.

$$\sum M_A = 0 \ \circlearrowleft +$$

$$R_B \cdot l - \frac{r}{2} \cdot l^2 + N_s \cdot e = 0 \Leftrightarrow$$

$$R_B = -\frac{N_s \cdot e}{l} + \frac{r}{2} \cdot l = -\frac{200\ \mathrm{N} \cdot 0.025\ \mathrm{m}}{2.3\ \mathrm{m}} + \frac{7.365\ \frac{\mathrm{N}}{\mathrm{m}}}{2} \cdot 2.3\ \mathrm{m} = 10.6437\ \mathrm{N}$$

$$\sum F_z = 0 \ \uparrow +$$

$$R_{A,1} + R_B - r \cdot l = 0 \Leftrightarrow$$

$$R_{A,1} = r \cdot l - R_B = 7.365 \frac{\mathrm{N}}{\mathrm{m}} \cdot 2.3\ \mathrm{m} - 10.6437\ \mathrm{N} = 6.2958\ \mathrm{N}$$

$$\sum F_x = 0 \ \rightarrow +$$

$$R_{A,2} = N_s = 200\ \mathrm{N}$$

[1] Tubes in accordance with this Standard are manufactured by cold forming and electric resistance pressure welding, cf. [W.1], 17/02-2011.

J.2.2 Distribution of bending moment

The distribution of the bending moment is calculated from Figure J.5.

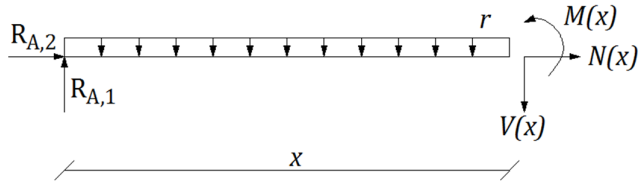

Figure J.5: Cut drawing.

$$\sum M = 0 \circlearrowleft +$$

$$M(x) + \frac{r}{2} \cdot x^2 - R_{A,1} \cdot x = 0 \Leftrightarrow$$

$$M(x) = 10.6437\ \mathrm{N} \cdot \mathrm{x} - \frac{7.365\ \frac{\mathrm{N}}{\mathrm{m}}}{2} \cdot x^2$$

The distribution of bending moment appears from Figure J.6.

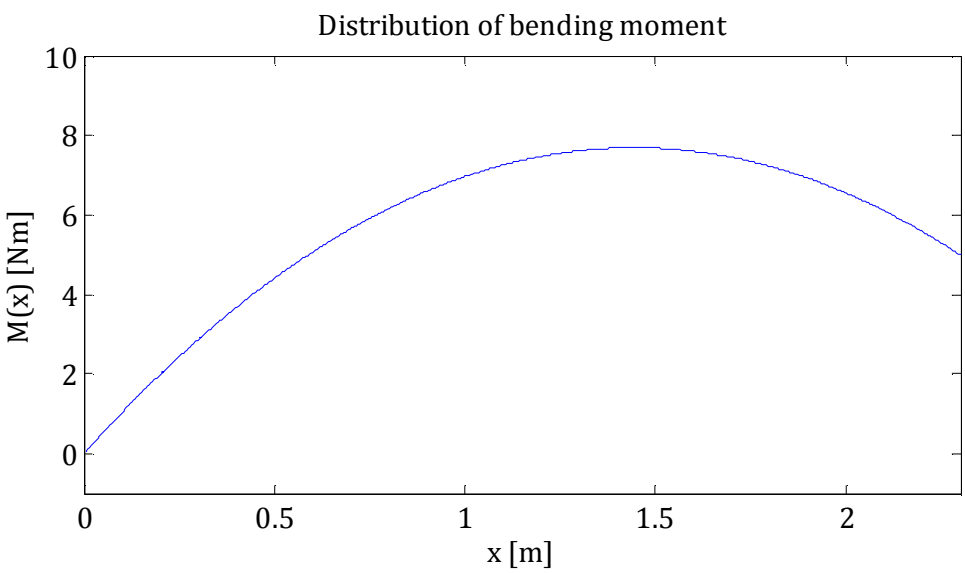

Figure J.6: Distribution of bending moment

$$M_{max} = M(x = 1.445\ \mathrm{m}) = 7.691\ \mathrm{Nm}$$

$$M_1 = M(x = 0\ \mathrm{m}) = 0\ \mathrm{Nm}$$

$$M_2 = M(x = 2.3\ \mathrm{m}) = 5\ \mathrm{Nm}$$

J.2.3 Control of bearing capacity in tension

The normal stress in the rod under affection of tension is calculated:

$$\varphi_N = \frac{N_s}{A} + \frac{M}{W_y} = \frac{200\ \mathrm{N}}{9.6 \cdot 10^{-5}\ \mathrm{m}^2} + \frac{5.127\ \mathrm{Nm}}{5.087 \cdot 10^{-7}\ \mathrm{m}^3} = 12.2\ \mathrm{MP} < \frac{235}{1.2}\mathrm{MP} = 195.8\ \mathrm{MP}$$

OKAY!

J.2.4 Control of bearing capacity in compression

When the rod is under affection of compression it is assumed to work as a strut and therefore the bearing capacity is reduced due to stability. Based on the Danish standard DS412 [7], the bearing capacity of the rod is sufficient if the following expression is fulfilled:

$$n_{max} + k_y m_y \leq 1 \tag{J.1}$$

Where:

$$n_{max} = \frac{N_s}{\chi \cdot A \cdot f_{yd}} \tag{J.2}$$

$$k_y = 1 - \mu_y \cdot n_{max} \leq 1.5 \tag{J.3}$$

$$m_y = \frac{M_s}{W_{pl} \cdot f_{yd}}, \text{in cross section class 1 and 2} \tag{J.4}$$

In equation (J.2):

$$\chi = \frac{1}{\phi + \sqrt{\phi^2 - \lambda^2}} \tag{J.5}$$

Where:

$$\phi = \frac{1}{2}(1 + \alpha(\lambda - \lambda_0) + \lambda^2) \tag{J.6}$$

and

$$\lambda = \frac{l_s / i_y}{89.4 \cdot \varepsilon} \tag{J.7}$$

In equation (J.6):

$$\lambda_0 = 0.2 \tag{J.8}$$

The imperfection factor, α, is determined from table look-up, e.g. [5] p. 133:

$$\alpha = 0.34 \tag{J.9}$$

In equation (J.7):

$$l_s = 1 \cdot l \text{, for simply supported struts, cf. [6] p. 140} \tag{J.10}$$

and

$$\varepsilon = \sqrt{\frac{f_{yd}\ [\text{MPa}]}{235\ \text{MPa}}} \tag{J.11}$$

In equation (J.3):

$$\mu_y = \lambda(2\beta_M - 4) + \delta_\mu \tag{J.12}$$

Where:

$$\beta_M = \beta_{M,\psi} + \frac{M_Q(\beta_{M,Q} - \beta_{M,\psi})}{\Delta M} \tag{J.13}$$

and

$$\delta_\mu = \frac{W_{pl} - W}{W} \text{, in cross section class 1 and 2} \tag{J.14}$$

In equation (J.13):

$$\Delta M = |M_{max}|\text{, because the sign of the bending moment does not change} \tag{J.15}$$

$$\beta_{M,\psi} = 1.8 - 0.7\psi\text{, in this particular case } \psi = 0 \text{ because } M_1 = 0 \tag{J.16}$$

$$\beta_{M,Q} = 1.3\text{, because } M_1 = 0 \tag{J.17}$$

$$M_Q = \left|M_{max,cross\ load}\right| \tag{J.18}$$

Where:

$$M_{max,cross\ load} \text{ is the maximum bending moment from the cross load only} \tag{J.19}$$

Cf. equation (J.10)

$$\lambda = \frac{l_s/i_y}{89.4 \cdot \varepsilon} = \frac{\frac{2.3\text{ m}}{0.0073\text{ m}}}{89.4 \cdot \sqrt{\frac{235/1.21}{235}}} = 3.8767$$

Cf. equation (J.6)

$$\phi = \frac{1}{2}(1 + 0.34(3.8767 - 0.2) + 3.8767^2) = 8.6394$$

Cf. equation (J.5)

$$\chi = \frac{1}{8.6394 + \sqrt{8.6394^2 - 3.8767^2}} = 0.0611$$

Cf. equation (J.2)

$$n_{max} = \frac{200\text{ N}}{0.0611 \cdot 9.6 \cdot 10^{-5}\text{ m}^2 \cdot \frac{235}{1.21} \cdot 10^6 \frac{\text{N}}{\text{m}^2}} = 0.1756$$

Cf. equation (J.13):

$$\beta_M = 1.8 + \frac{\frac{1}{8} r l^2 (1.3 - 1.8)}{7.691\text{ Nm}} = 1.8 + \frac{-\frac{1}{16} \cdot 7.365 \cdot 2.3^2\text{ Nm}}{7.691\text{ Nm}} = 1.4834$$

Cf. equation (J.12) :

$$\mu_y = 3.8767(2 \cdot 1.4834 - 4) + \frac{6.33 \cdot 10^{-7} - 5.087 \cdot 10^{-7}\text{ m}^3}{5.087 \cdot 10^{-7}\text{ m}^3} = -4.881$$

Cf. equation (J.3):

$$k_y = 1 - \mu_y \cdot n_{max} = 1 + 4.881 \cdot 0.1756 = 1.8571 \Rightarrow$$
$$k_y = 1.5$$

Cf. equation (J.4):

$$m_y = \frac{M_s}{W_{pl} \cdot f_{yd}} = \frac{7.691\ \text{Nm}}{6.33 \cdot 10^{-7}\ \text{m}^3 \cdot \frac{235 \cdot 10^6 \frac{\text{N}}{\text{m}^2}}{1.21}} = 0.0626$$

$$0.1756 + 1.5 \cdot 0.0626 = 0.2703 \leq 1$$

OKAY!

The profile is stronger towards bending around its y-axis than it is around its z-axis. Therefore the profile bearing capacity is controlled for stability in the xy-plane as well.

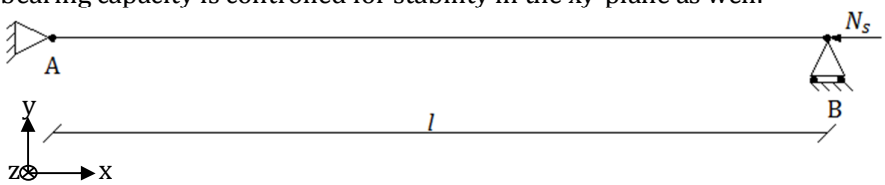

Figure J.7: Static system for connecting rod in xy-plane.

For a simply supported strut with no bending moment, see Figure J.7, the bearing capacity is controlled by equation (J.2).

$$n_{max} = \frac{N_s}{\chi \cdot A \cdot f_{yd}} \leq 1$$

Here χ is different from before since λ is different due to differences between i_y and i_x.

$$\lambda = \frac{l_s / i_x}{89.4 \cdot \varepsilon} = \frac{\frac{2.3\ \text{m}}{0.0058\ \text{m}}}{89.4 \cdot \sqrt{\frac{235/1.21}{235}}} = 4.8793$$

$$\phi = \frac{1}{2}(1 + 0.34(4.8793 - 0.2) + 4.8793^2) = 13.1993$$

$$\chi = \frac{1}{13.1993 + \sqrt{13.1993^2 - 4.8793^2}} = 0.0393$$

$$n_{max} = \frac{200\ \text{N}}{0.0393 \cdot 9.6 \cdot 10^{-5}\text{m}^2 \cdot \frac{235}{1.21} \cdot 10^6\ \frac{\text{N}}{\text{m}^2}} = 0.273 < 1$$

OKAY!

K. Methods of restraining the pile

In the cyclic experiments in dry sand it is observed that the pile moves upward during the experiments. In this appendix, the examination of different solution methods for this problem is described.
The first solution that we thought of was to place some weight on top of the pile.

K.1 Weight on top of the pile

A system to hold the weight on top of the pile is designed. It consists of a bolt fastened to two pieces of angle iron which grab around the pile top. A bolt goes though the angle irons and the pile so that the system doesn't rotate. The system is pictured on top of the pile in Figure K.1.

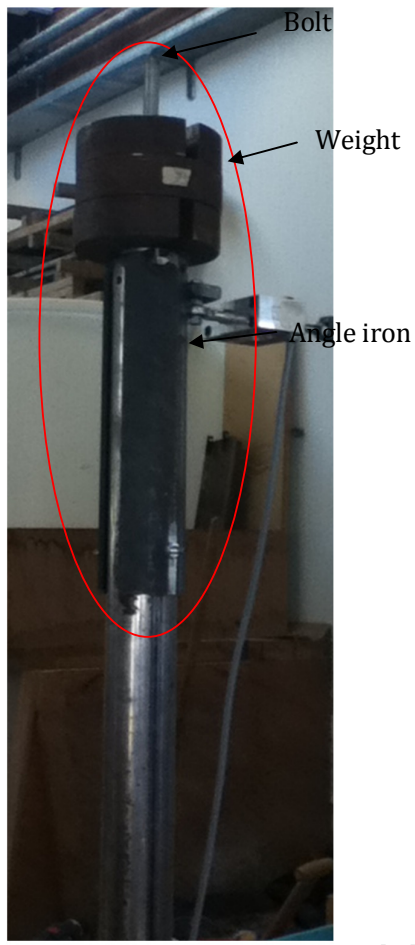

Figure K.1: The system for putting weight on top of the pile marked with a red ellipse.

The amount of weight which is necessary to put on top of the pile so that it neither moves upward or downward is unknown. Therefore different amounts are tried and at the end it seems like the perfect amount is found. The box is packed with sand again and the weight is put on top of the pile. When the cyclic load is applied the pile moves downward about 1 cm, which is acceptable, but after about an hour of loading, the sand has compacted around the pile, causing is to move upward and keep moving upward.
The conclusion of this examination is therefore that the weight on top of the pile has to be adjustable during the experiments. This is impossible to achieve using this system.

K.2 Straps

Straps are fastened to the pile, perpendicular to the loading direction and then fastened to the box. The system with the straps is shown in Figure K.2.

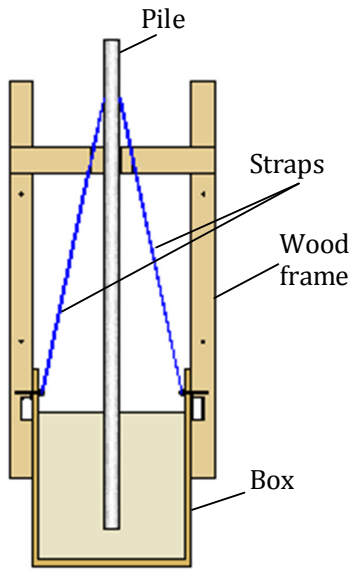

Figure K.2: Experimental setup for cyclic pile experiments using straps for restraining the pile from moving upward.

The idea of the straps is that the they are self-adjusting. When the pile downward the straps are loosened and the pile starts moving upward. The straps are then tightened causing the pile to move downward again. This means that the vertical movement of the pile can be controlled within one cm. This is acceptable; therefore the solution with the straps is used in the experiments

L. Results of cyclic experiments

In this appendix the results of the cyclic tests are shown and the results of the repetitions are compared in order to verify the test results' validity.

L.1 Results of tests in dry sand

In this section the results of the tests in dry sand for the three different frequencies are shown and the repetitions for each frequency are compared.

L.1.1 Results for frequency of 0.27 Hz

Figure L.1 to Figure L.3 show the load as a function of the number of cycles for the three repetitions of the cyclic tests with a loading frequency of 0.27 Hz.

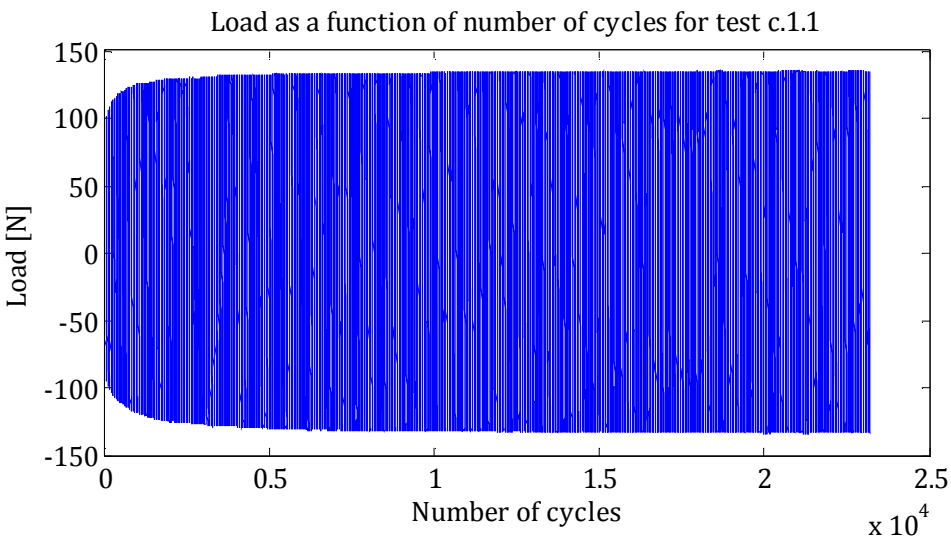

Figure L.1: Load as a function of the number of cycles for cyclic test c.1.1.

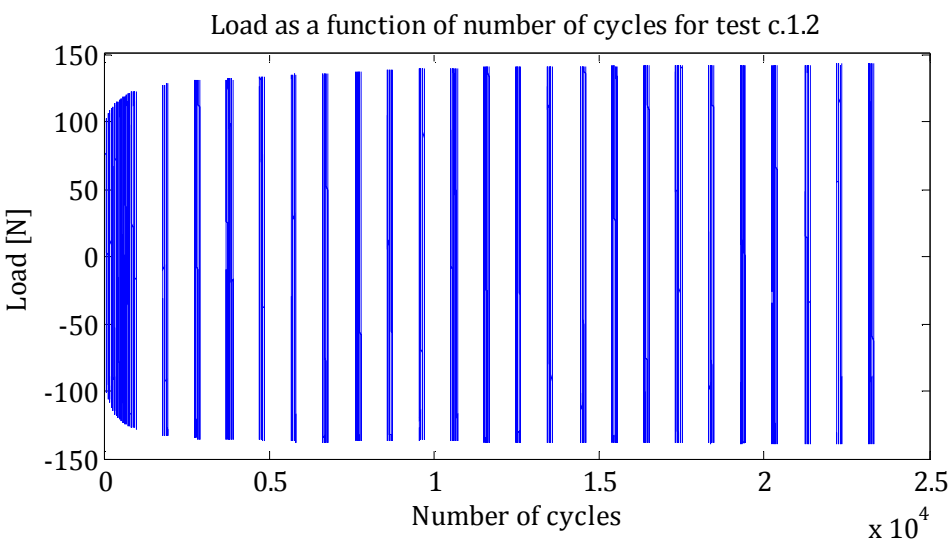

Figure L.2: Load as a function of the number of cycles for cyclic test c.1.2.

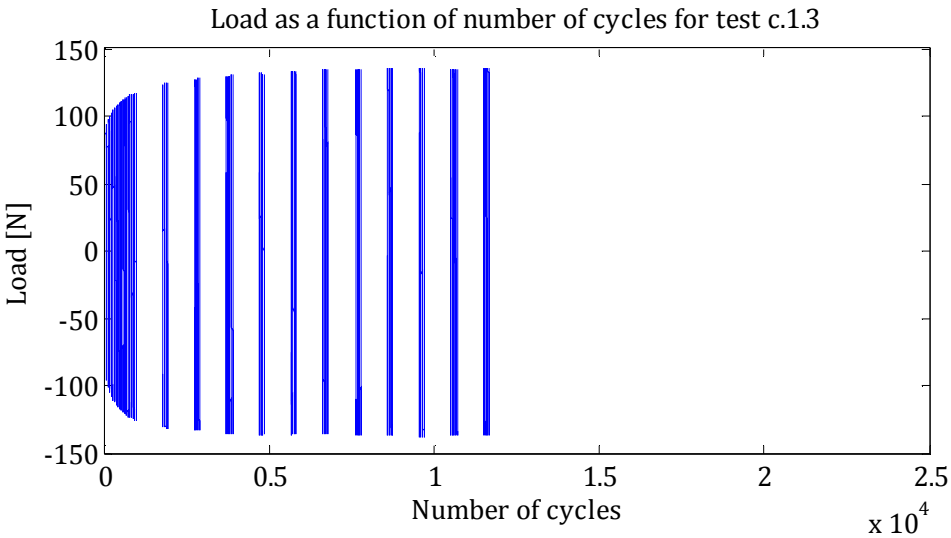

Figure L.3: Load as a function of the number of cycles for cyclic test c.1.3.

It is seen from the three figures that the development of the force with the number of cycles and the value of the force is very similar. Test c.1.1 shows a smaller force than the two other tests, which can be caused by either the compactness of the soil around the pile or the pile moving upward or downward during the test. For the very first cycles the force in test c.1.3 is smaller than the other two tests. This is caused by a difference in the compactness of the sand at at the beginning of the experiment. It is assessed that the results are similar enough to be considered credible.

L.1.2 Results for frequency of 0.56 Hz

Figure L.4 and Figure L.5 show the load as a function of the number of cycles for the two repetitions of the cyclic tests with a loading frequency of 0.56 Hz.

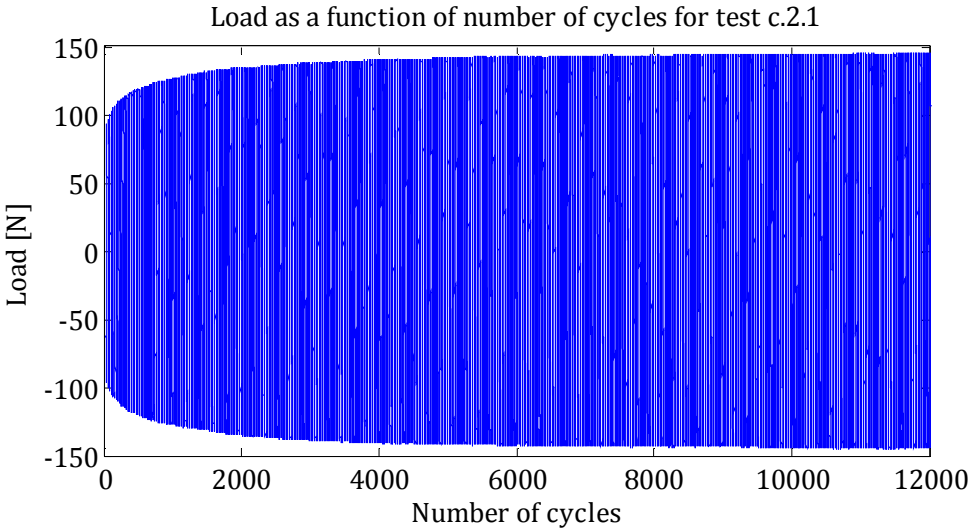

Figure L.4: Load as a function of the number of cycles for cyclic test c.2.1.

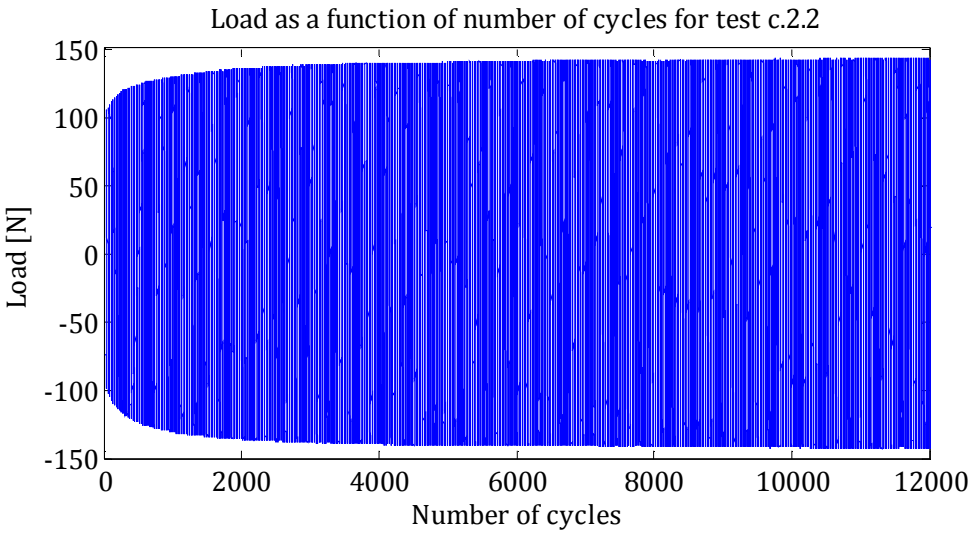

Figure L.5: Load as a function of the number of cycles for cyclic test c.2.2.

It is seen from the two figures that the results of the two tests are very similar and therefore for test results are considered credible.

L.1.3 Results for frequency of 0.84 Hz

Figure L.6 and Figure L.7 show the load as a function of the number of cycles for the two repetitions of the cyclic tests with a loading frequency of 0.84 Hz.

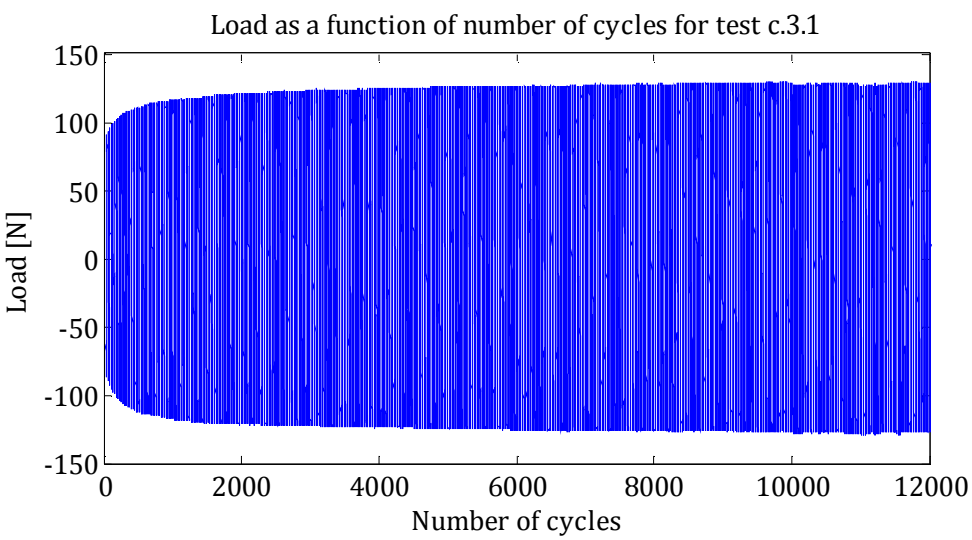

Figure L.6: Load as a function of the number of cycles for cyclic test c.3.1.

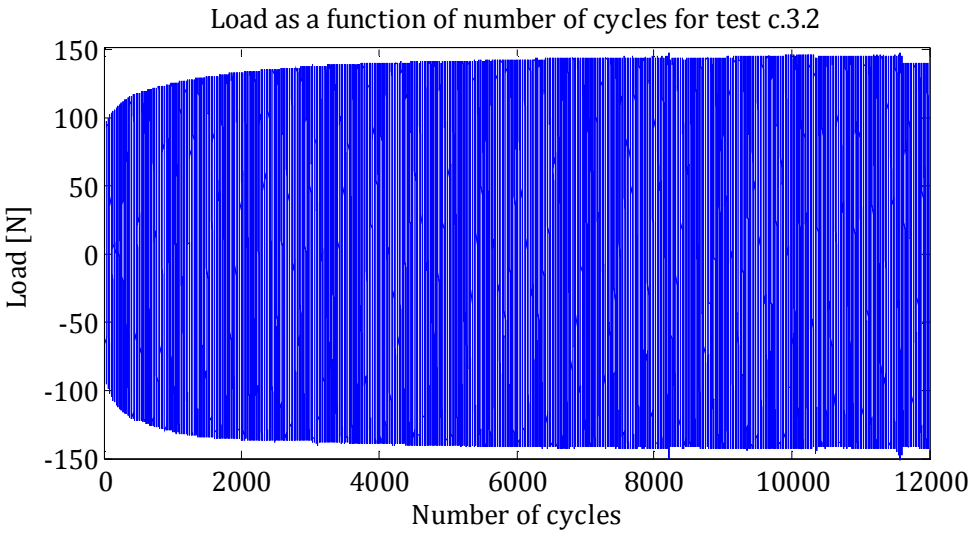

Figure L.7: Load as a function of the number of cycles for cyclic test c.3.2.

It is seen from the two figures that the force is larger for test c.3.2 than it is for test c.3.1. This can be explained by the pile moving upward in test c.3.1 causing the force to become smaller. The foundation depth at the end of test c.3.1 is 0.38 m and for test c.3.2 the depth is 0.395 m. So when this is taken into account when using the results, they can be considered credible.

M. Material models in Abaqus

To develop a 3D model of the pile in Abaqus it is essential that a realistic material model for the sand is used. Abaqus includes a material model called Mohr Coulomb plasticity. This incorporated material model and a user defined material model, also based on the Mohr-Coulomb theory, are examined in this section.

M.1 Theoretical solutions

The Abaqus model for testing the two material models for the sand is compared to a theoretical solution. Therefore a centrally loaded circular footing is modelled as theoretical solutions for this is known. The dimensions of the footing are shown in

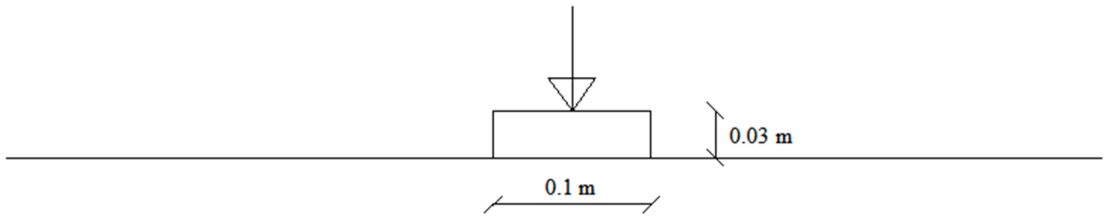

Figure M.1: Centrally loaded circular footing made of steel with a diameter of 0.1 m and a height of 0.03 m.

The bearing capacity of a circular footing can be calculated with the general bearing capacity formula, cf. [M.2], Lærebog I geoteknik:

$$\frac{R'}{A'} = \frac{1}{2} \cdot \gamma \cdot b' \cdot N_\gamma \cdot s_\gamma \cdot i_\gamma + q' \cdot N_q \cdot s_q \cdot i_q + c' \cdot N_c \cdot s_c \cdot i_c \tag{M.1}$$

Where:

γ is the effective density of the soil [N/m²]
b' is the effective width of the footing [m]
A' is the effective area of the footing [m²]
R' is the effective bearing capacity [N]
c' is the effective cohesion of the soil [N/m²]
q' is the effective surface load beside the footing [N/m²]
N_γ, N_q and N_c are bearing capacity factors
s_γ, s_q and s_c are shape factors
i_γ, i_q and i_c are gradient factors

The footing is centrally loaded and therefore the effective dimensions of the footing are the geometric dimensions.

The bearing capacity factors, N_q and N_c, can be determined by the expressions:

$$N_q = e^{\pi \cdot tan(\varphi)} \cdot \frac{1 + sin(\varphi)}{1 - sin(\varphi)} \tag{M.2}$$

$$N_c = \frac{N_q - 1}{tan(\varphi)} \tag{M.3}$$

The shape factors for N_q and N_c can be determined as:

$$s_q = s_c = 1 + 0.2 \cdot \frac{b'}{l'} \tag{M.4}$$

The gradient factors are determined as:

$$i_\gamma = i_q^2 \tag{M.5}$$

$$i_q = i_c = \left(1 - \frac{H}{V + A' \cdot c' \cdot cot(\varphi)}\right) \tag{M.6}$$

Where:
H is the horizontal load [N]
V is the vertical load [N]
l' is the effective length of the footing [m]
φ is the friction angle [°]

The bearing capacity factor for the density, N_γ, cannot be exactly determined and the calculation differs depending on the source. In Eurocode 7, cf. [M.1] the expression for N_γ for strip- and point footings is:

$$N_\gamma = 2 \cdot (N_q - 1) \cdot tan(\varphi) \tag{M.7}$$

In [M.2], p. 224 the expression for N_γ can be applied to both square, circular and oval footings. The expression is:

$$N_\gamma = \frac{1}{4} \cdot \left((N_q - 1) \cdot cos(\varphi)\right)^{\frac{3}{2}} \tag{M.8}$$

The expression is conservative compared to equation (M.7).
In [M.1] and in [M.2] the shape factor, s_γ, is also given. In [M.2] the expression is not dependent of the shape of the footing, where in [M.1] the expression depends on the shape of the footing. The shape factors for a circular footing according to the two sources are:

$$s_\gamma = 1 - 0.4 \cdot \frac{b'}{l'} = 0.6 \qquad \text{[M.2]} \tag{M.9}$$

$$s_\gamma = 0.7 \qquad \text{[M.1]} \tag{M.10}$$

In an article written by D.J. White et al [M.3] the bearing capacity of circular footings on sand is discussed. The authors compare different expressions for N_γ both for strip footings and circular footings. In this article an alternative expression for N_γ is presented. This expression can be applied only to circular footings, with no shape factor:

$$N_\gamma = 0.0286 \cdot e^{0.2109 \cdot \varphi} \tag{M.11}$$

The bearing capacities for the footing in Figure M.1 is calculated in Table M-1 to Table M-3, using equation (M.1) with the three different expression for N_γ

It is stated that equation (M.11) is valid for completely rough footings where it is not stated in the sources whether equation (M.7) and (M.8) are valid for rough or smooth footings.

Lærebog i geoteknik [M.2]												
c [Pa]	φ [°]	γ [N/m³]	N_γ	N_q	N_c	s_γ	s_q	s_c	i_γ	i_q	i_c	R [N]
1000	40	17,540	84.2	64.2	75.3	0.6	1.2	1.2	1	1	1	1058
100	40	17,540	84.2	64.2	75.3	0.6	1.2	1.2	1	1	1	418
10	40	17,540	84.2	64.2	75.3	0.6	1.2	1.2	1	1	1	355
0	40	17,540	84.2	64.2	75.3	0.6	1.2	1.2	1	1	1	348

Table M-1: Bearing capacities calculated with equation(M.1) for different values of the cohesion. The expression for N_γ is equation (M.8).

Eurocode 7 [M.1]												
c [Pa]	φ [°]	γ [N/m³]	N_γ	N_q	N_c	s_γ	s_q	s_c	i_γ	i_q	i_c	R [N]
1000	40	17,540	106	64.2	75.3	0.7	1.2	1.2	1	1	1	1221
100	40	17,540	106	64.2	75.3	0.7	1.2	1.2	1	1	1	585
10	40	17,540	106	64.2	75.3	0.7	1.2	1.2	1	1	1	518
0	40	17,540	106	64.2	75.3	0.7	1.2	1.2	1	1	1	511

Table M-2: : Bearing capacities calculated with equation(M.1) for different values of the cohesion. The expression for N_γ is equation (M.7).

D.J. White et al [M.3]												
c [Pa]	φ [°]	γ [N/m³]	N_γ	N_q	N_c	s_γ	s_q	s_c	i_γ	i_q	i_c	R [N]
1000	40	17,540	132	64.2	75.3	1.0	1.2	1.2	1	1	1	1618
100	40	17,540	132	64.2	75.3	1.0	1.2	1.2	1	1	1	979
10	40	17,540	132	64.2	75.3	1.0	1.2	1.2	1	1	1	915
0	40	17,540	132	64.2	75.3	1.0	1.2	1.2	1	1	1	908

Table M-3: : Bearing capacities calculated with equation(M.1) for different values of the cohesion. The expression for N_γ is equation (M.11).

It can be seen that for cohesionless soil the method of determining N_γ has great influence on the bearing capacity. The value of N_γ is much higher when using equation (M.11) than when the other two expressions are used. This can be because the expression is valid for completely rough foundations.
The calculated bearing capacities are used to compare to the results of the Abaqus model with the two different material models.

M.2 Geometry of the finite element model

The geometry of the model in Abaqus is shown in figure m.2. The finite element model consists of a soil domain where the circular footing is placed on top. The footing is centrally loaded which means that both symmetry around the x- and y-axis can be utilized. The width and length of the soil domain is chosen to be ten times the diameter of the foundation. Therefore the dimensions of the soil domain in the model are 0.5×0.5 m. The height of the soil domain is 0.5 m as well, resulting in a cubic soil domain.

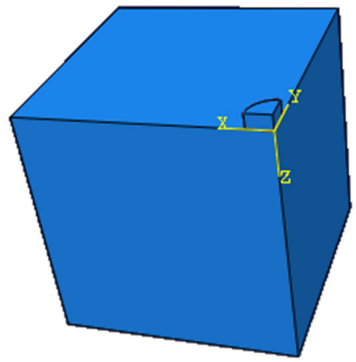

Figure M.2: Illustration of the circular foundation modeled in Abaqus.

M.2.1 Interaction between footing and soil domain

The interaction between the footing and the soil domain can be modelled using a coefficient of friction or as fully bonded.
In the model for examination of the user defined material model the interaction is fully bonded and in the model for examination of the incorporated material model the interaction is frictional.
When modelling the interaction using a coefficient of friction "hard" contact [2] with slip after contact is applied normal to the direction of the load. The tangential behaviour is defined as penalty[3] with a coefficient of friction μ = 0.4.
The method of applying friction is examined for a simple case, where the friction between a block subjected to a lateral movement and a base is examined. The block is subjected to a normal force of 0.0025 N and the coefficient of friction between the block and the base has a value of 0.4. Thus the reaction when moving the block is:

$$R = 0.4 \cdot P_N = 0.001\ N$$

The force-displacement curve from the examination appears from Figure M.3.

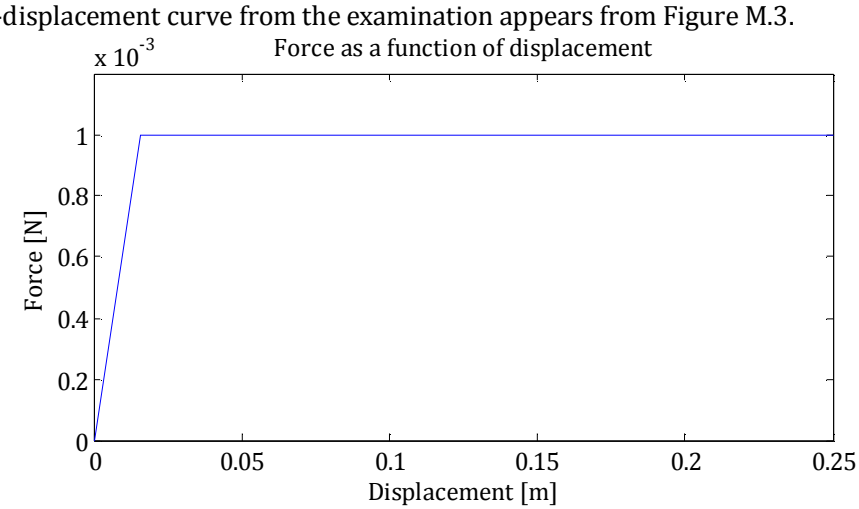

Figure M.3: Force as a function of displacement determined from an Abaqus model of a block moving on a fricional base.

[2] When applying "Hard" contact the elements will press on each other rather than move into each other. When applying slip after contact the elements will let go when the two surfaces are pulled away from each other.
[3] The penalty method is a method where a constrained equation is divided into a series of unconstrained equations, whose solution converges towards the original constraint

The reaction force when the curve is horizontal is 0.001 N which means the friction between the block and the base works as expected.

M.3 Boundary conditions

The constraint surfaces in the model are the symmetry surfaces, the side surfaces and the bottom of the soil domain, see figure m.4.

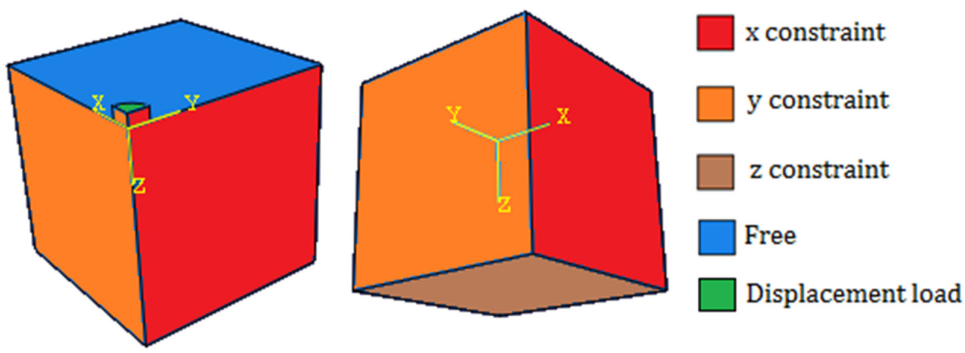

Figure M.4: Boundary conditions for the Abaqus model of a circular footing.

The load on the footing is a uniformly distributed displacement in the z-direction.

M.4 Mesh

The mesh used in the examination is shown in Figure M.5.

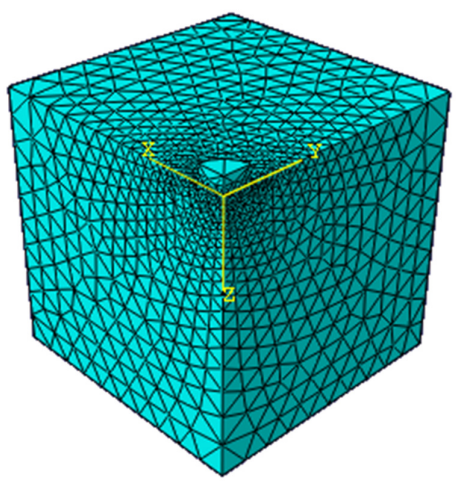

Figure M.5: Illustration of the mesh.

M.4.1 Geostatic step

The overburden pressure increases with increasing depth, This means that the weight of the sand must be included in the model. When the gravity is activated in the model displacements in the soil is introduced. These displacements can cause disturbance of the analysis. This is taken into account in a geostatic step where initial stresses are calculated for the soil domain. These stresses have the same values but with opposite signs of the stresses coming from the gravity load. Therefore the total stresses and displacements will be equal to zero at the end of the geostatic step.

The initial stresses are determined in a FORTRAN script where the vertical initial stresses are computed from:

$$\sigma_z = \gamma \cdot d \tag{M.12}$$

where

d is the depth [m]
γ is the density of the soil [kg/m³]

The stresses perpendicular to the vertical stresses are determined as:

$$\sigma_x = \gamma \cdot d \cdot K_0 \tag{M.13}$$

$$\sigma_y = \gamma \cdot d \cdot K_0 \tag{M.14}$$

where:

$K_0 = 1 - sin(\varphi)$ is the earth pressure coefficient at rest

The displacements at the end of the geostatic step with the gravity load not activated appear from figure m.6 to the left. To the right are the displacements at the end of the geostatic step with the gravity load activated.

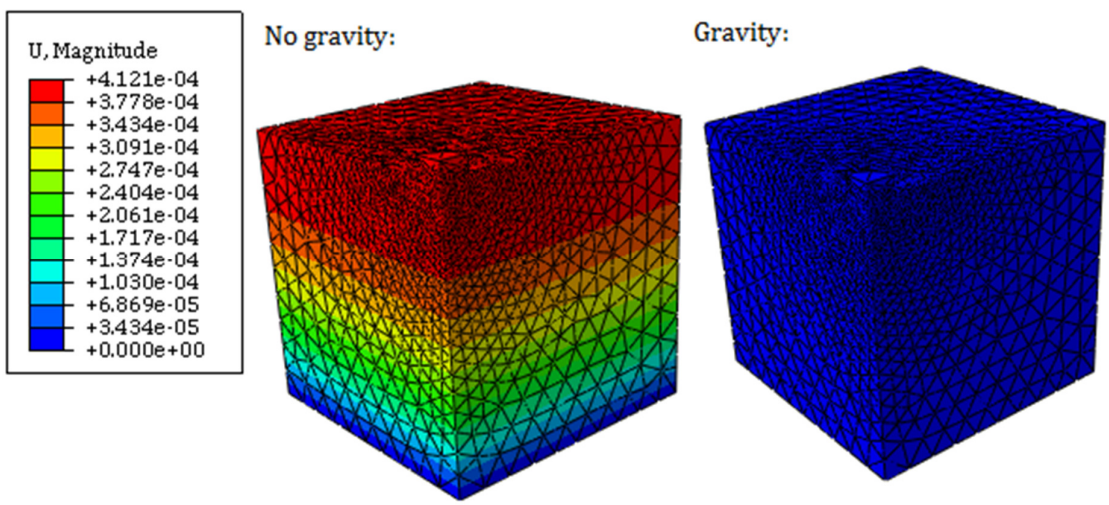

Figure M.6: Displacements in the model at the end of the geostatic step with no gravity load to the left. To the right: Displacements at the end of the geostatic step with the gravity load activated. When the gravity load is active the displacements has a magnitude of $1 \cdot 10^{-10}$ m. The displacements on the figure are in m.

It is evident from the figure that the displacements are close to zero at the end of the geostatic step.

M.5 User defined Mohr-Coulomb material model

A user defined Mohr-Coulomb material model is examined in this section.
The material model is based on the Mohr-Coulomb theory. The input parameters are young's modulus, Poisson's ratio, the cohesion, the angle of friction and the angle of dilation.
The calculated results are based on associated plasticity since using diverse values for the angle of friction and the angle and dilatation causes problems with convergence.

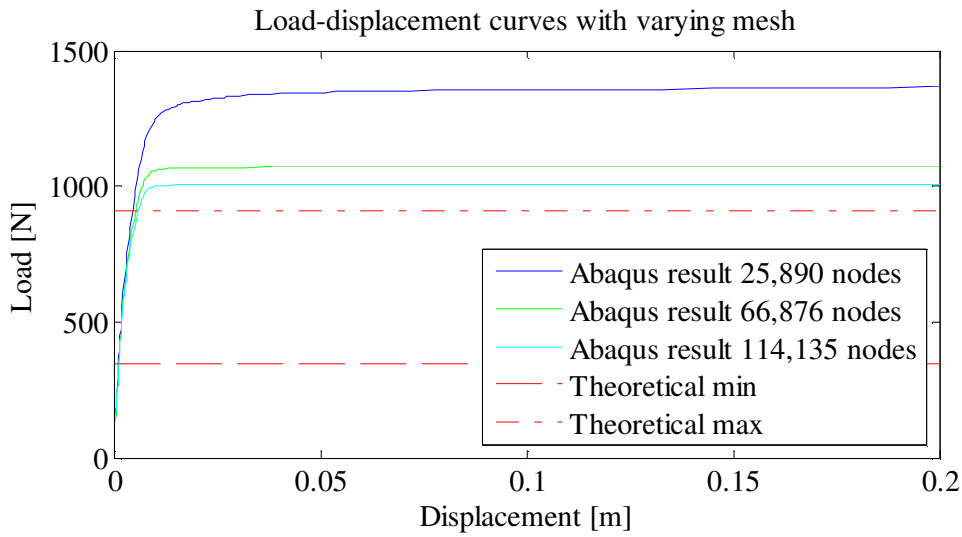

Figure M.7: Force-displacement curves for the footing with different meshes

M.6 Incorporated Mohr-Coulomb material model

The Mohr-Coulomb plasticity model which is incorporated in Abaqus is examined in this section. The cohesion cannot be zero in this material model, why the model is examined for different values of the cohesion and the results are compared with theoretical solutions. The interaction between the footing and the soil domain is friction with a coefficient of friction of 0.4.
The load displacement curves and the theoretical results appear from Figure M.8 through Figure M.10. It appears from Figure M.8 that the analysis is aborted by Abaqus before there is fracture in the soil.

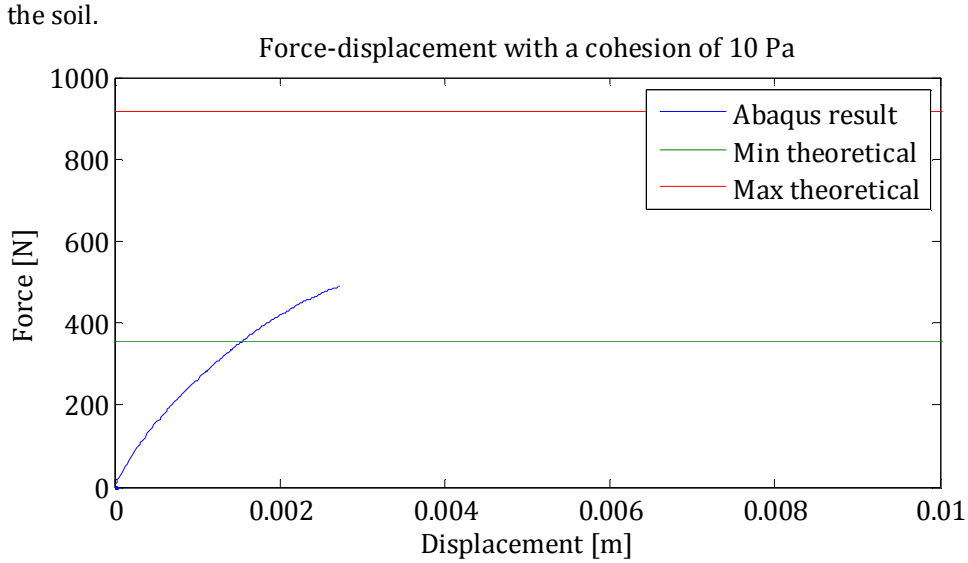

Figure M.8: Load-displacement curve from analysis with a cohesion of 10 Pa.

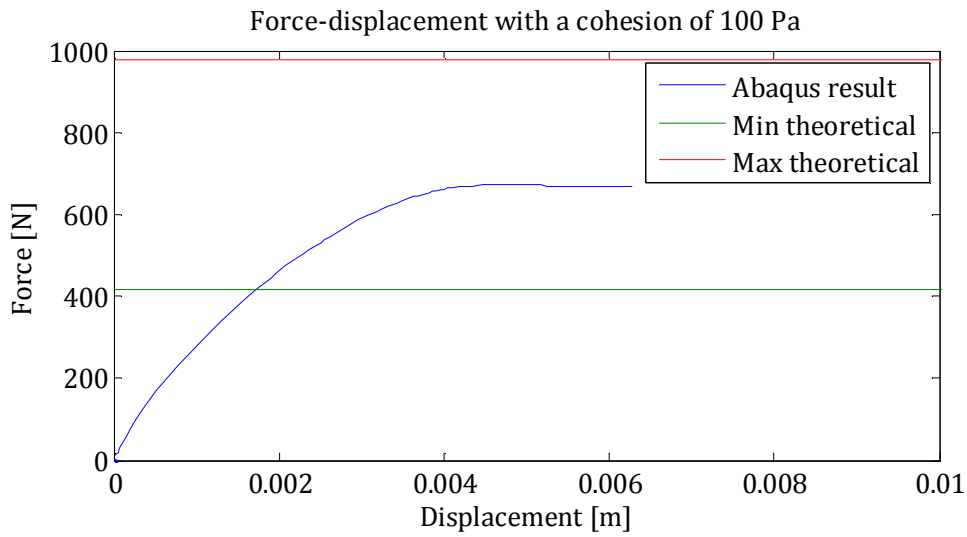

Figure M.9: Load-displacement curve from analysis with a cohesion of 100 Pa.

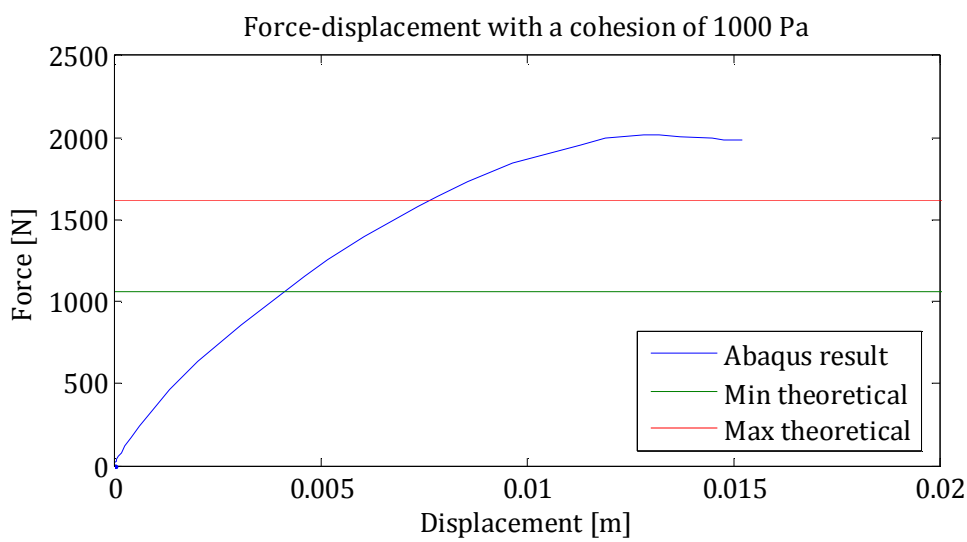

Figure M.10: Load-displacement curve from analysis with a cohesion of 1000 Pa.

M.7 Conclusion

The user defined material model shows good results and the analyses run stably even though the value of the cohesion is zero. The incorporated material model in Abaqus does not accept for the value of the cohesion to be zero and when the value is set very small the analysis does not run stably and is aborted before the ultimate resistance is reached. Therefore it is concluded that the user defined material model is most suitable for modelling sand and this material model is chosen to model the experimental pile.

M.8 References

[M.1] Eurocode 7: Geotechnical design – Part 1: General rules
DS/EN 1997-1
2nd edition, 2007-06-22
Danish standards

[M.2] Lærebog i geoteknik
Redaktion: Niels Krebs Ovesen, Leif Fuglsang and Gunnar Bagge
Polyteknisk

[M.3] *A comparison of the bearing capacity of flat and conical circular foundations on sand*
White, D. J., Teh, K. L., Leung, C. F. & Chow, Y. K.
(2008). Géotechnique 58, No. 10, 781–792 [doi: 10.1680/geot.2008.3781]